AFOSR 1493 SID 61-275

BOUNDARY LAYER TRANSITION AT SUPERSONIC SPEEDS—THREE DIMENSIONAL ROUGHNESS EFFECTS (SPHERES)

15 August 1961

by

E. R. van Driest and C. B. Blumer
Space Sciences Laboratory

NORTH AMERICAN AVIATION, INC.
SPACE and INFORMATION SYSTEMS DIVISION

FOREWORD

The investigation described in this report was supported by the United States Air Force through the Office of Scientific Research of the Office of Aerospace Research under Contract AF 49(638)-250.

ABSTRACT

Further experiments carried out in the 12-inch supersonic wind tunnel of the Jet Propulsion Laboratory of the California Institute of Technology to investigate the effect of three-dimensional roughness elements (spheres) on boundary-layer transition on a 10-degree (apex angle) cone without heat transfer are reported herein. The local Mach number for these tests was 2.71. The data show clearly that the minimum (effective) size of trip required to bring transition to its lowest Reynolds number varies as the one-fourth power of the distance from the apex of the cone to the trip. Use of available data at other Mach numbers indicates that the Mach number influence for effective tripping is taken into account by the simple expression

$$Re_{\delta^*} = 1025 \left(1 + \frac{\gamma-1}{2} M_\delta^2\right) (k/\delta^*)^{-2}.$$

Some remarks concerning the roughness variation for transition on a blunt body are made. Finally, a general criterion is introduced which gives insight to the transition phenomenon and anticipates effects of external and internal disturbances, Mach number, and heat transfer.

CONTENTS

	Page
INTRODUCTION	1
EXPERIMENTAL APPARATUS	3
ANALYSIS OF DATA	5
Cones and Flat Plates	5
Blunt Bodies	14
General	15
NOMENCLATURE	18
REFERENCES	20

ILLUSTRATIONS

Figure		Page
1	View of 10° Cone in Supersonic Wind Tunnel	22
2	Methods of Mounting Spherical Roughness Elements on Cone (a) Tip Roughness Mounting, (b) Band Roughness Mounting	23
3	Typical Magnified Schlieren Photographs of Transition on Smooth Adiabatic Cone, $M_\delta = 2.71$	24
4	The Variation of Transition Location With Unit Reynolds Number on a Cone, $M_\delta = 2.71$	25
5(a)	The Variation of Transition Reynolds Number With Trip Reynolds Number on a Cone, $M_\delta = 2.71$	26
5(b)	The Variation of Transition Reynolds Number With Trip Reynolds Number on a Cone, $M_\delta = 2.71$	27
5(c)	The Variation of Transition Reynolds Number With Trip Reynolds Number on a Cone, $M_\delta = 2.71$	28
5(d)	The Variation of Transition Reynolds Number With Trip Reynolds Number on a Cone, $M_\delta = 2.71$	29
5(e)	The Variation of Transition Reynolds Number With Trip Reynolds Number on a Cone, $M_\delta = 2.71$	30
5(f)	The Variation of Transition Reynolds Number With Trip Reynolds Number on a Cone, $M_\delta = 2.71$	31
5(g)	The Variation of Transition Reynolds Number With Trip Reynolds Number on a Cone, $M_\delta = 2.71$	32
5(h)	The Variation of Transition Reynolds Number With Trip Reynolds Number on a Cone, $M_\delta = 2.71$	33
5(i)	The Variation of Transition Reynolds Number With Trip Reynolds Number on a Cone, $M_\delta = 2.71$	34
5(j)	The Variation of Transition Reynolds Number With Trip Reynolds Number on a Cone, $M_\delta = 2.71$	35
5(k)	The Variation of Transition Reynolds Number With Trip Reynolds Number on a Cone, $M_\delta = 2.71$	36
5(l)	The Variation of Transition Reynolds Number With Trip Reynolds Number on a Cone, $M_\delta = 2.71$	37
5(m)	The Variation of Transition Reynolds Number With Trip Reynolds Number on a Cone, $M_\delta = 2.71$	38
5(n)	The Variation of Transition Reynolds Number With Trip Reynolds Number on a Cone, $M_\delta = 2.71$	39
6	Summary of Roughness Induced Transition Data on a Cone $M_\delta = 2.71$	40

Figure		Page
7	Effective Trip Position Reynolds Number on a Cone Versus Trip Reynolds Number for Various Mach Numbers	41
8	Effective Displacement-Thickness Transition Reynolds Number Versus k/δ^* for Various Mach Numbers	42
9	Composite Plot of Spherical Roughness Data for Various Mach Numbers	43
10	The Variation of Effective Transition Reynolds Number With Trip Number on a Cone, $M_\delta = 2.71$	44
11	Schematic Diagram of the Velocity Profile in the Region of the Disturbing Element	45
12	The Relative Height of Effective Trips in a Laminar Boundary Layer at $M_\delta = 2.71$	46
13	Interval Between Transition and Effective Roughness Elements as a Function of Mach Number	47
14	The Variation of Effective Trip Reynolds Number With Trip Number on a Cone, $M = 2.71$.	48

INTRODUCTION

Boundary-layer transition continues to remain prominent in the field of fluid dynamics, because of its decisive effect on many practical problems such as aerodynamic drag, heat transfer, and lately, radar cross-section of re-entering bodies. Research on transition implies research on flow instability whether in a laminar boundary layer or in the viscous sublayer of a fully turbulent flow. An understanding of the latter process would lead to solutions of the turbulent boundary layer with favorable and adverse pressure gradients, blowing and suction, and magnetic effects.

The mechanism of transition can be studied by introduction of finite disturbances into the boundary layer flow and observation of the ensuing process. Experiments of this type are described in this paper using spherical roughness elements to disturb the flow on a 10-degree cone at local Mach number 2.71 at the outer edge of the boundary layer. A practical consequence of these experiments is the determination of the minimum size of single elements required to bring transition to its lowest Reynolds number relative to the disturbing element. Comparison of data presented here with data collected previously at other Mach numbers shows the effect of compressibility. No heat transfer is involved in these studies.

The paper represents a considerable extension of previous work in Refs. 1 and 2 in that it brings together a broader range of experimental data on

transition induced by single roughness elements, particularly at local Mach number 2.71, and gives a more complete analytical treatment.

EXPERIMENTAL APPARATUS

The tests were carried out in the 12-inch supersonic wind tunnel of the Jet Propulsion Laboratory (CIT) using the smooth 20-inch, 10-degree cone illustrated in Fig. 1. The wind tunnel and cone model are described in Ref. 2.

In the present experiments, the position of the roughness elements from the apex of the cone was varied from approximately 0.5 inches to 8.6 inches. The roughness elements used were accurately ground steel spheres with nominal diameters of 0.005, 0.0075, 0.010, 0.015 inches. These spheres were cemented with epoxy resin either to replaceable conical tips or to thin bands which were in turn fitted to the model. Typical tip and band ball mountings are shown in Fig. 2. The surface discontinuity caused by the band thickness (0.0025 inch or less) had a negligible effect on the data for roughness stations five inches or more from the cone tip; however, this discontinuity could not be tolerated nearer to the cone tip so these roughness configurations were fabricated directly on a set of matched three-inch-long tips (Fig. 2). Previous tests showed that a roughness spacing of 4k was sufficient to insure no interaction between roughness elements. The roughness element height of completed trips was measured with a precision micrometer to the number of significant figures indicated in the legend of Fig. 5; however, the actual values presented are averages with maximum variations of ± 2 percent in roughness height tolerated. The variation in number of significant figures is a result of

several of the earlier trips being destroyed before the high precision measuring equipment was obtained.

Transition was detected by means of the magnified schlieren system developed for this work. This device, which magnified the schlieren image of the boundary layer 20 times normal to the flow, was adequate for the entire range of Reynolds numbers covered in the experiments. Typical magnified schlieren pictures of the movement of transition with change in Reynolds number per inch are shown in Fig. 3. The average accuracy of reading the transition position from data films was ± 0. 1 inches. In general the reading accuracy was better when transition was forward on the cone (i. e. when the unit Reynolds number was large) and poorer when transition was far aft on the cone.

ANALYSIS OF THE DATA

Cones and Flat Plates

A dimensional analysis of the important variables involved in the disturbance-produced transition process will be useful in establishing the principal dimensionless coordinates which will in turn facilitate the derivation of significant results. The primary variables for a zero pressure gradient flow may be expressed functionally as

$$x_t = x_t\,(\rho_\delta,\ u_\delta, \mu_\delta,\ x_k,\ k,\ M_\delta,\ \text{free-stream disturbances}) \qquad (1)$$

in which x_t is transition position and ρ_δ, u_δ, μ_δ, M_δ are as usual the density, velocity, viscosity, and Mach number at the outer edge of the boundary layer. k is the size of the roughness element and x_k is the distance to the trip from the cone apex. In terms of dimensionless quantities, this equation then takes the form,

$$\frac{\rho_\delta\, u_\delta\, x_t}{\mu_\delta} = f\left(\frac{\rho_\delta\, u_\delta\, x_k}{\mu_\delta},\ \frac{\rho_\delta\, u_\delta k}{\mu_\delta},\ M_\delta,\ \begin{array}{l}\text{dimensionless}\\ \text{free-stream}\\ \text{disturbances}\end{array}\right). \qquad (2)$$

It is the purpose of the reported investigation to study the effect on transition of disturbances produced by surface roughness elements, in this case specifically surface-mounted spherical roughness elements. To simplify the analysis, it was desirable to make the experiments relatively independent of the effects of free-stream disturbances. This was done (as illustrated in Fig. 4) by placing the roughness elements sufficiently far forward of the

smooth wall transition (i. e. sufficiently far forward of transition produced by free-stream disturbances). Fig. 4 is a typical plot of transition position x_t in inches as a function of Reynolds number per inch $\rho_\delta u_\delta/\mu_\delta$ in terms of conditions at the outer edge of the boundary layer. The movement of transition when the wall is smooth is indicated by curve 4 in the figure. When a ring of spherical elements of size k is placed at position x_k the movement of transition takes the course as indicated by curves 1, 2, and 3 successively as the unit Reynolds number is increased. (The unit Reynolds number is changed by changing the pressure in the wind tunnel.) The relative roles played by disturbances from the roughness elements and the free stream are readily indicated. In zone 1, the free stream disturbances are predominant in establishing transition, whereas in zone 3 the roughness element predominates in locating transition. In zone 2, the roughness element has become large enough relative to the boundary-layer thickness to produce a drastic forward movement of transition; however, the effect of free-stream disturbances must still be considered in this region.

Of particular interest to the following analysis is the intersection between zones 2 and 3, the effective point. More precisely a trip is defined as effective in this paper when the Reynolds number of transition $\rho_\delta u_\delta x_t/\mu_\delta$ is a minimum. At this condition the influence of free-stream disturbances is considered negligible. If one also restricts the experiment to constant Mach number, Eq. 2 then becomes

$$\frac{\rho_\delta u_\delta x_t}{\mu_\delta} = f\left(\frac{\rho_\delta u_\delta x_k}{\mu_\delta}, \frac{\rho_\delta u_\delta k}{\mu_\delta}\right) \tag{3}$$

Equation 3 can be written in an equivalent form, viz.,

$$\frac{\rho_\delta u_\delta x_t}{\mu_\delta} = f\left(\frac{x_k}{k}, \frac{\rho_\delta u_\delta k}{\mu_\delta}\right) \tag{4}$$

which is of more direct interest because it is the manner in which the experiments were conducted and the resulting data plotted, i. e., for a fixed geometrical condition (disturbance element size k at a certain location x_k on the cone) the Reynolds number of the transition position $\rho_\delta u_\delta x_t/\mu_\delta$ was observed as the Reynolds number of the trip $\rho_\delta u_\delta k/\mu_\delta$ was varied, see Figs. 5(a) through 5(n). The ratio x_k/k will be called the trip number in this paper. Therefore, for the same trip number, the transition Reynolds number should be a single function of the trip Reynolds number. That this is indeed the case is seen specifically in Figs. 5(c), (d), (g), (m), and (n). Each plot presents data for a single trip number but with various sized trips and corresponding trip positions.

It can now be shown that for effective trip Reynolds numbers the influence of free-stream disturbances is indeed negligible. First, it is observed in Fig. 5 that the smooth wall transition Reynolds number, which is a measure of the free-stream disturbance level, varied from about 3.0×10^6 to 4.6×10^6 for the present experiments (note: the smooth wall transition Reynolds number was only a function of wind tunnel unit Reynolds number). Next, it is seen in Figs. 5(c), (d), (g), (m), and (n), where a direct

comparison may be made, that no appreciable effect of free-stream disturbance on the effective transition Reynolds number exists.

Although not directly related to the present analysis, it is of interest to examine the variation of zone 1 with trip number. At large values of trip number it is seen (Fig. 5) that the data lie very close to the smooth wall transition curve and it may be concluded that the free-stream disturbances establish transition. However, as the trip number decreases, the separation between smooth wall transition and zone 1 transition increases, thus indicating that both wall and stream disturbances play a part in fixing transition. It is further noted that the transition Reynolds number of the corner between zones 1 and 2 is dependent upon the corresponding smooth wall transition Reynolds number as well as on the trip number.

A phenomenon which is not completely understood is the inflection that occurs in zone 3 of the roughness-induced transition curve near $Re_k = 3000$ for small trip numbers. This peculiarity becomes more pronounced with a decrease in trip number as is evident in Figs. 5(a) through 5(f) for trip numbers between 67 and 333.

Figure 6 summarizes all of the transition data for Mach number $M_\delta = 2.71$, the solid lines for each x_k/k representing a fairing of the data presented in Fig. 5. The circles at the low points of these faired curves indicate the minimum transition Reynolds numbers for each roughness configuration which were previously defined as the effective transition Reynolds numbers. Some of the faired curves in Fig. 6 have been deleted for clarity, but all of the

effective points as read from the data of Fig. 5 are presented. Where several trip configurations possessed nearly the same trip number, i. e., Fig. 5(c) or 5(d), an average was computed and a single value of effective Re_t and Re_k was read. The effective trip position Reynolds numbers Re_{x_k} which correspond to the effective transition Reynolds numbers are shown as diamonds in Fig. 6. Although discussed later, it is noted in passing that effective transition occurs a constant Reynolds numbers increment behind the roughness element.

The shape of the Re_{x_k} vs Re_k curve for effective tripping (see Fig. 6) can be deduced. It is first assumed that the local conditions at the trip are responsible for the destruction of the laminar flow. It follows that there is a local Reynolds number of the trip which must remain constant for effective tripping. Thus, for incompressible flow, $\rho u_k k/\mu$ = constant, where u_k is the velocity in the undisturbed laminar boundary layer at the height of the trip. Therefore, in the region of linear velocity profile there would result

$$Re_k \sim Re_{x_k}^{1/4} \tag{5}$$

which for a given boundary layer reduces to

$$k \sim x^{1/4} \tag{6}$$

For compressible flow the locations at which the density ρ and viscosity μ of the local Reynolds number are evaluated must be specified. However, any suitable choice of density and viscosity will produce a relation of the form

$$Re_k \sim f(M_\delta) \cdot Re_{x_k}^{1/4} \tag{7}$$

which indeed appears to hold true as seen when Eq. 7 is fitted to the diamonds in Fig. 6.

In a first attempt to determine the Mach number function $f(M_\delta)$ in Eq. 7, a local Reynolds number was evaluated using density ρ_k and viscosity μ_k at the height of the trip. However, this local Reynolds number did not prove to remain constant for effective tripping. Rather, it was found that an artificial Reynolds number based on the density in the free stream and the viscosity at the wall, i.e., $\rho_\delta u_k k/\mu_w$, and with Pr = 1 and $\rho\mu$ = constant, yielded an expression which did fit data at various Mach numbers, namely,

$$Re_k \sim (1 + \frac{\gamma-1}{2} M_\delta^2) \cdot Re_{x_k}^{1/4} . \qquad (8)$$

The constant for Eq. 8 was established by fitting the data of Fig. 6 and the resulting formula for cone flow is

$$Re_k = 32.8 (1 + \frac{\gamma-1}{2} M_\delta^2) \cdot Re_{x_k}^{1/4} \quad \text{(cone)}. \qquad (9)$$

The corresponding equation for flow on a flat plate is

$$Re_k = 43.2 (1 + \frac{\gamma-1}{2} M_\delta^2) \cdot Re_{x_k}^{1/4} \quad \text{(plate)}. \qquad (10)$$

It is next of particular interest to compare the data of this paper at M_δ = 2.71 with data at other Mach numbers in order to evaluate the validity of the Mach number term in the above equations. Such data are available for flow on a cone at Mach numbers 1.90 and 3.67 in Ref. 2 and for flow on a flat plate at Mach number zero in Ref. 3. The supersonic cone data of Ref. 2 and the present paper are compared directly with Eq. 9 in Fig. 7. The dashed Mach number zero curve in the figure is presented for reference only.

In order to compare the data for plates and cones, it is necessary to consider the boundary layer Reynolds number at the trip in terms of a local length such as the displacement thickness δ^* rather than the development (history) length x_k. Data from Ref. 2 and 3 are then plotted in Fig. 8 along with the data of the present paper using the boundary layer Reynolds number Re_{δ^*} at the trip at effective tripping. The abscissa of Fig. 8 has been taken as k/δ^* according to Dryden[4]. Furthermore, since δ^* is also a function of Mach number, i.e., for a flat plate $Re_{\delta^*} = 1.73 \left(1 + \frac{\gamma-1}{2} M_\delta^2\right) \cdot Re_x^{1/2}$ which is accurate within 5 percent for $0 \leq M \leq 5$, Eq. 8 becomes

$$Re_{\delta^*} = 1025 \left(1 + \frac{\gamma-1}{2} M_\delta^2\right) (k/\delta^*)^{-2}. \qquad (11)$$

Again, the constant has been evaluated by matching the $M_\delta = 2.71$ data. Encouragingly enough, all of the data for effective spherical roughness elements including $M_\delta = 0$ are in quite good agreement with Eq. 11. Hence, if the abscissa of Fig. 8 is taken as $\left(1 + \frac{\gamma-1}{2} M_\delta^2\right)^{-1/2} \cdot (k/\delta^*)$, all of the data for spheres should collapse, as indeed they do in Fig. 9.

A practical form for the direct determination of the minimum (effective) size of disturbing elements (spheres) required to promote transitions at a certain position and Reynolds number on an aircraft model or the maximum size of elements allowable on a prototype may be obtained by rearranging Eq. 9 or 10. For cone flow Eq. 9 yields

$$x_k/k = \frac{Re_{x_k}^{3/4}}{32.8 \left(1 + \frac{\gamma-1}{2} M_\delta^2\right)} \qquad \text{(cone)}. \qquad (12)$$

which is shown with the $M_\delta = 2.71$ data in Fig. 10.

Returning to the initial assumption of a constant local trip Reynolds number as the transition criterion, it is found from Eq. 11 that

$$\frac{\rho u_k k}{\mu} = 588 \qquad \text{(spheres)} \qquad (13)$$

for incompressible flat plate flow. This number is in good agreement with results obtained by Klebanoff, et al, in Ref. 3 and von Doenhoff in Ref. 5. More generally, however, a trip Reynolds number which holds for supersonic flow is $\rho_\delta u_k k/\mu_w = 588$ with $Pr = 1$ and $\rho\mu$ = constant.

It should be noted that data from Tani (Ref. 6) for two-dimensional disturbance elements (wires) at $M_\delta = 0$ are also plotted in Fig. 8, again using only the effective points as previously defined. Although the latter data are not sufficient to draw a firm conclusion, it is expected that a relationship again like $Re_{\delta^*} \sim f(M_\delta) \cdot (k/\delta^*)^{-2}$ will also hold for two-dimensional disturbance elements. Indeed from the figure it appears that $Re_{\delta^*} = 465\,(k/\delta^*)^{-2}$ and that

$$\frac{\rho u_k k}{\mu} = 267 \qquad \text{(wires)} \qquad (14)$$

for $M_\delta = 0$. This lower value of local effective trip Reynolds number compared to that for spheres is presumably due to the fact that the two-dimensional disturbance element creates a larger velocity overshoot than the sphere (see Fig. 11).

The above analysis is concerned with the development of a relationship between trip size and location for effective tripping; however, it is observed in Fig. 6 and even more clearly in Fig. 10 that the effective transition location is some distance downstream of the trip at Mach number $M_\delta = 2.71$. In fact, it is quite evident in Fig. 10 that transition occurs a constant Reynolds number increment behind the roughness element, i.e., for $M_\delta = 2.71$,

$$Re_t = Re_{x_k} + 0.5 \times 10^6 \tag{15}$$

for values of $x_k/k > 200$. Upon consideration of the local flow pattern about the disturbance element for supersonic boundary layers, and in the present experiments the spheres always protruded into the supersonic portion of the boundary layer as shown in Fig. 12, this delay in transition is indeed to be expected owing to the overexpansion of the gas over the spheres and consequent holding of the disturbance to the surface behind the spheres. Therefore, it is also to be expected that the delay in transition when the trip is effective will increase with Mach number. That this is true is seen in Fig. 13 using the data from Refs. 2, 3, and 7 and the present paper. It is to be noted, however, that in Fig. 13 the subsonic data of Ref. 3 are for spherical roughness elements on a flat plate, and the hypersonic data of Ref. 7 are for transition caused by wind tunnel wall contamination also on a flat plate. Interestingly enough, the data of Ref. 7 appear to follow the trend of the spherical roughness data. The practical importance of the delay in transition is obvious, particularly at very high Mach numbers. Thus it is possible that,

The above analysis is concerned with the development of a relationship between trip size and location for effective tripping; however, it is observed in Fig. 6 and even more clearly in Fig. 10 that the effective transition location is some distance downstream of the trip at Mach number $M_\delta = 2.71$. In fact, it is quite evident in Fig. 10 that transition occurs a constant Reynolds number increment behind the roughness element, i.e., for $M_\delta = 2.71$,

$$Re_t = Re_{x_k} + 0.5 \times 10^6 \tag{15}$$

for values of $x_k/k > 200$. Upon consideration of the local flow pattern about the disturbance element for supersonic boundary layers, and in the present experiments the spheres always protruded into the supersonic portion of the boundary layer as shown in Fig. 12, this delay in transition is indeed to be expected owing to the overexpansion of the gas over the spheres and consequent holding of the disturbance to the surface behind the spheres. Therefore, it is also to be expected that the delay in transition when the trip is effective will increase with Mach number. That this is true is seen in Fig. 13 using the data from Refs. 2, 3, and 6 and the present paper. It is to be noted, however, that in Fig. 13 the subsonic data of Ref. 3 are for spherical roughness elements on a flat plate, and the hypersonic data of Ref. 6 are for transition caused by wind tunnel wall contamination also on a flat plate. Interestingly enough, the data of Ref. 6 appear to follow the trend of the spherical roughness data. The practical importance of the delay in transition is obvious, particularly at very high Mach numbers. Thus it is possible that,

even though a trip may be effective, the ensuing transition may occur a considerable distance downstream.

The divergence of the effective transition Reynolds number from Eq. 15 as x_k/k becomes small, can be qualitatively explained with the aid of Fig. 12, which is a scale drawing of the laminar boundary layer on a cone with M_δ = 2.71 showing the variation in effective trip height with trip number. For values of $x_k/k > 200$ the effective trip is substantially within the linear portion of the velocity profile and good agreement with the analysis is experienced. However, for smaller values of trip number the trip extends above the linear velocity profile region and no longer meets this assumption of the analysis, so it should not be surprising that the data separate from the analytical curve. It is important to observe that the minimum transition Reynolds number produced by a single band of spherical roughness elements at the Mach number of the present experiments is about $Re_{t_{min}} = 10^6$ as shown in Fig. 6. Further, the data indicate that a lower limit on trip Reynolds number exists, namely, $Re_{k_{min}} \approx 1500$, as the roughness elements become appreciably larger than the boundary layer, i.e., as $x_k/k \to 0$, see Fig. 14.

Blunt Bodies

A remark can be made about roughness-induced transition on blunt bodies. Since the local velocity near the stagnation point increases directly with distance x from that point, it follows for constant free-stream Reynolds number that in the stagnation region

$$k \sim x^{-1/2}. \tag{16}$$

Hence, on the face of a blunt body, the size of roughness for effective tripping decreases with increasing distance from the stagnation point, as compared with an increase with $x^{1/4}$ on a cone or flat plate. Furthermore, if properties are evaluated at the edge of the boundary layer in the vicinity of the disturbing element the form of Eq. 5 applies directly. Experiments to determine the constant of Eq. 5 for blunt bodies are now in progress under the present Air Force Office of Scientific Research contract.

General

Although the above analysis permitted the development of certain relationships for roughness size to induce transition, it is clear that a more general approach to the transition phenomena is necessary to anticipate the effects of pressure gradient, heat transfer, mass transfer, and free-stream turbulence. In quest of a more fundamental criterion for transition, comparison is made of the turbulent and viscous terms in the boundary layer equation for mean turbulent flow, under the basic premise that the flow becomes fully turbulent when the inertial terms are sufficiently large compared to the viscous terms, whereupon

$$\frac{\epsilon}{\mu} = \frac{\rho l^2}{\mu} \cdot \frac{du}{dy} = \text{const.} \qquad (17)$$

which is the ratio of the eddy viscosity ϵ to the molecular viscosity μ. The letter l is the Prandtl mixing length and du/dy the mean velocity gradient. For flow along a smooth wall, this ratio[8] is about 24.

Assuming that $l = Ky$, Eq. 17 becomes

$$K^2 \cdot \frac{\rho y^2}{\mu} \cdot \frac{du}{dy} = \text{const.} \tag{18}$$

or

$$\frac{\rho y^2}{\mu} \cdot \frac{du}{dy} = \text{const.} = Tr. \tag{19}$$

This expression, which represents the beginning of the fully turbulent flow velocity profile, or the end of the viscous influence of the wall, has a value $24/(0.4)^2 = 150$, for $K = 0.4$. If $l = Ky$ is considered general, then Eq. 19 will hold for all kinds of turbulent interfaces, including blowing, etc. For purposes of computation, however, the flow near a wall is usually assumed to consist of a purely laminar sublayer which suddenly breaks down to turbulent flow. The edge of the sublayer may then be computed using Eq. 19 applied to the laminar flow condition, but with a constant of 128 as determined from velocity profiles in smooth pipes. This criterion has been used with success in obtaining the thickness of the sublayer and subsequent solution of the turbulent boundary layer problem with blowing and suction[9] and is expected to open the way for solution with pressure gradient and magnetic effects.

It is finally assumed that Eq. 19 can be applied to a laminar boundary layer to indicate impending breakdown to turbulence, that is, transition. The criterion then states physically that the vorticity must be sufficiently "separated" from the wall to allow free tumbling against viscous restraint. A simple relation for the effect of free-stream disturbance on transition including external pressure gradient now follows approximately,

$$\frac{Tr}{Re_{\delta_t}} = A - B\Lambda$$

$$= A - B\,(\bar{\Lambda}+\Lambda')$$

$$= A + B\,\frac{\delta^2}{u_\delta \mu}\,\frac{dp}{dx} + B\,\frac{\delta^2}{u_\delta \mu}\,\left(\frac{dp}{dx}\right)' \qquad (20)$$

$$= A + B\,\frac{\delta^2}{u_\delta \mu}\,\frac{dp}{dx} + C\,Re_{\delta_t}^{\,2}\,\left(\frac{1}{Re_\lambda}\right)\left(\frac{u'}{u_\delta}\right)^2$$

where $\bar{\Lambda}$ and Λ' are the mean value and fluctuation in the Pohlhausen parameter, respectively, $Re_\lambda = \rho u_\delta \lambda/\mu$ with λ = eddy size in the free stream, and u' = root-mean-square velocity fluctuation in the free stream. Hence, an increase in disturbance $(dp/dx)'$ causes a decrease in Re_{δ_t}. Note also in Eq. 20 that a negative dp/dx as exhibited by a blunt body stabilizes the flow. When applied further to a compressible boundary layer, Eq. 19 gives a decrease in transition Reynolds number with increase in Mach number for insulated flow, and a delay in transition with cooling.

NOMENCLATURE

k	roughness element height
K	mixing length constant
l	Prandtl mixing length
M	Mach number
Pr	Prandtl number
p	pressure
Re_k	Reynolds number of trip, $\rho_\delta u_\delta k/\mu_\delta$
Re_t	Reynolds number of transition, $\rho_\delta u_\delta x_t/\mu_\delta$
Re_{x_k}	Reynolds number of trip position, $\rho_\delta u_\delta x_k/\mu_\delta$
Re_{δ^*}	Reynolds number based on displacement thickness, $\rho_\delta u_\delta \delta^*/\mu_\delta$
Re_{δ_t}	Reynolds number of transition based on boundary layer thickness, $\rho_\delta u_\delta \delta_t/\mu_\delta$
Re_λ	Reynolds number based on eddy size, $\rho u_\delta \lambda/\mu$
Tr	Transition number (Eq. 19), $(\rho y^2/\mu).\frac{du}{dy}$
u	velocity
x	length along cone surface measured from apex
x_k/k	trip number
y	length perpendicular to surface measured from surface
γ	ratio of specific heats
δ	boundary layer thickness

δ^*	boundary layer displacement thickness
ϵ	eddy viscosity
λ	eddy size
Λ	Pohlhauser parameter
μ	fluid viscosity
ρ	fluid density

SUBSCRIPTS

k	conditions at roughness element
eff	effective
t	transition
x_k	length along cone surface from apex to roughness element
δ	conditions at edge of boundary layer
δ^*	displacement thickness

REFERENCES

1. van Driest, E. R., and Blumer, C. B., "Effect of Roughness on Transition in Supersonic Flow," AGARD Report 255, April, 1960.

2. van Driest, E. R., and McCauley, W. D., "The Effect of Controlled Three-Dimensional Roughness on Boundary Layer Transition at Supersonic Speeds," Journal of the Aero-Space Sciences, Vol. 27, No. 4, pp. 261-271, April, 1960.

3. Klebanoff, P. S., Schubauer, G. B., and Tidstrom, K. D., "Measurements of the Effect of Two-Dimensional and Three-Dimensional Roughness Elements on Boundary Layer Transition," Journal of the Aeronautical Sciences, Vol. 22, No. 11, pp. 803-804, November, 1955.

4. Dryden, H. L., "Review of Published Data on the Effect of Roughness on Transition From Laminar to Turbulent Flow," Journal of the Aeronautical Sciences, Vol. 20, No. 7, pp. 477-482, July, 1953.

5. von Doenhoff, A. E., and Horton, E. A., "A Low-Speed Experimental Investigation of the Effect of a Sandpaper Type of Roughness on Boundary Layer Transition," NACA Report 1349, 1958.

6. Tani, I. Hama, F. R., and Mituisi, S., "On the Effect of a Single Roughness Element on Boundary Layer Transition," Report of the Institute of Sciences and Technology, University of Tokyo, Vol. 8, No. 3, pp. 124-133, May, 1954.

7. Korkegi, R. H., "Transition Studies and Skin Friction Measurements on an Insulated Flat Plate at a Mach Number of 5.8," Journal of the Aeronautical Sciences, Vol. 23, No. 2, pp. 97-107, February, 1956.

8. van Driest, E. R., "On Turbulent Flow Near a Wall," Journal of the Aeronautical Sciences, Vol. 23, No. 11, pp. 1007-1011, November, 1956.

9. van Driest, E. R., "On the Aerodynamic Heating of Blunt Bodies," ZAMP, Vol. IXb, pp. 223-248, March 17, 1958.

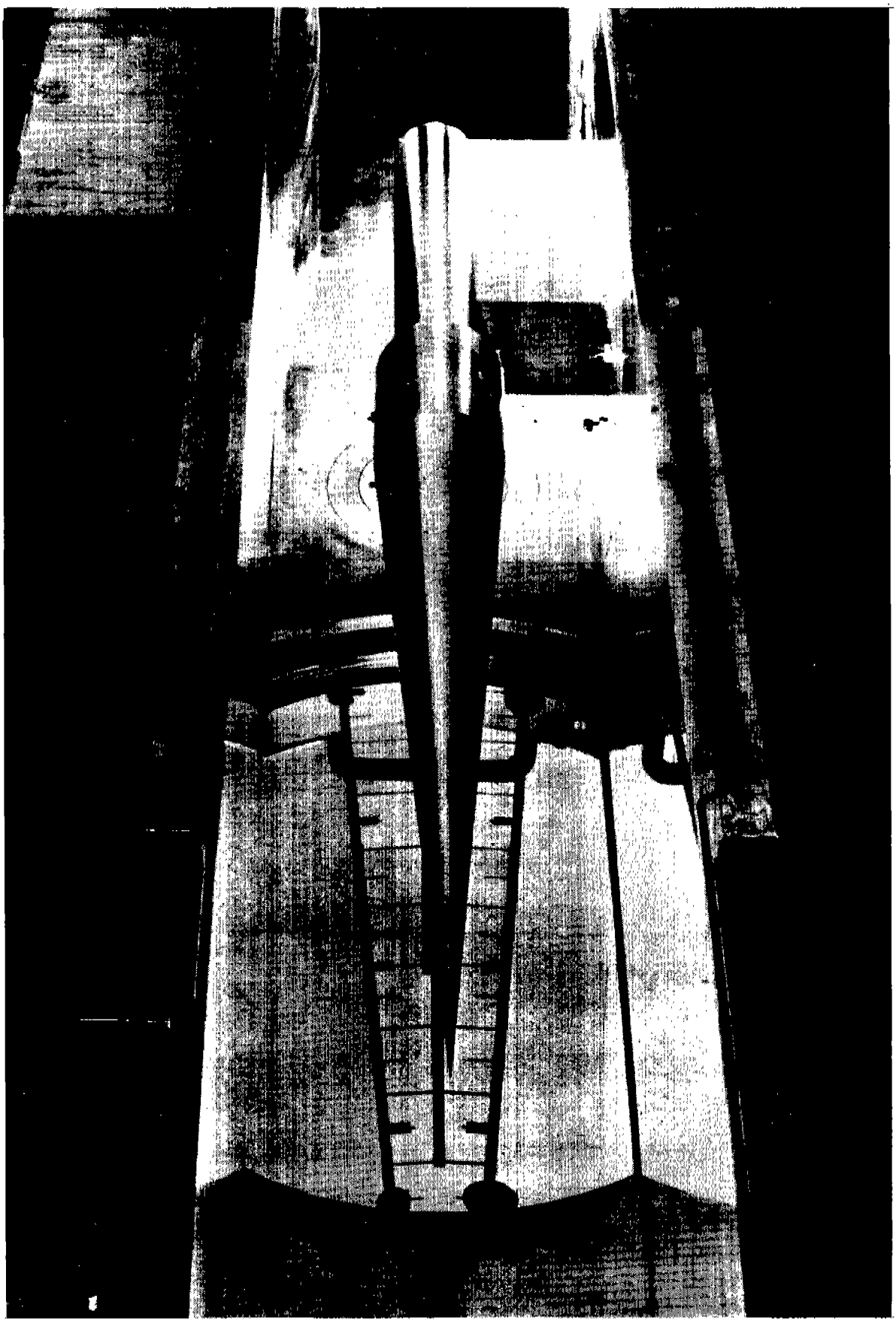

Figure 1. View of 10° Cone in Supersonic Wind Tunnel

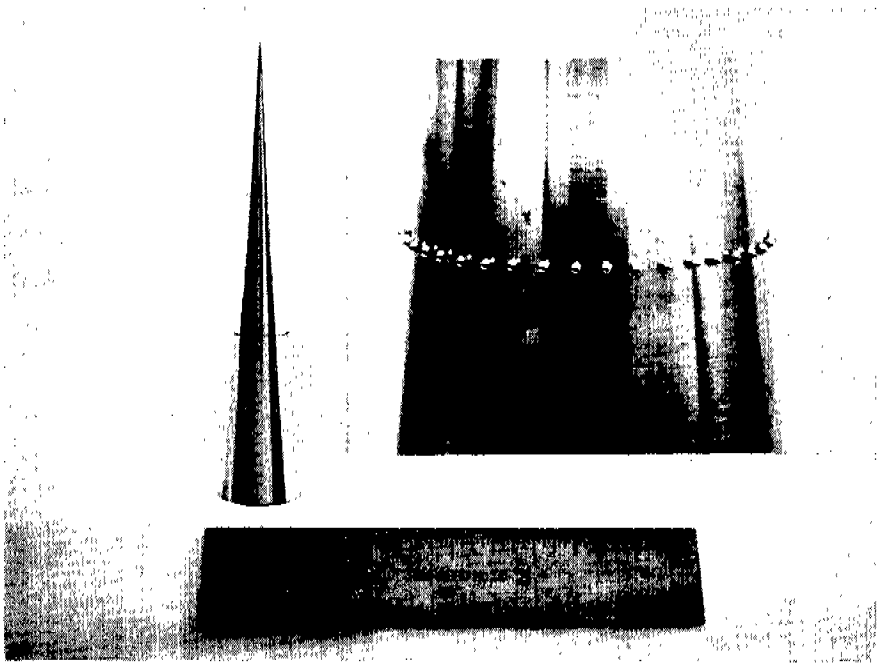

(a) TIP ROUGHNESS MOUNTING

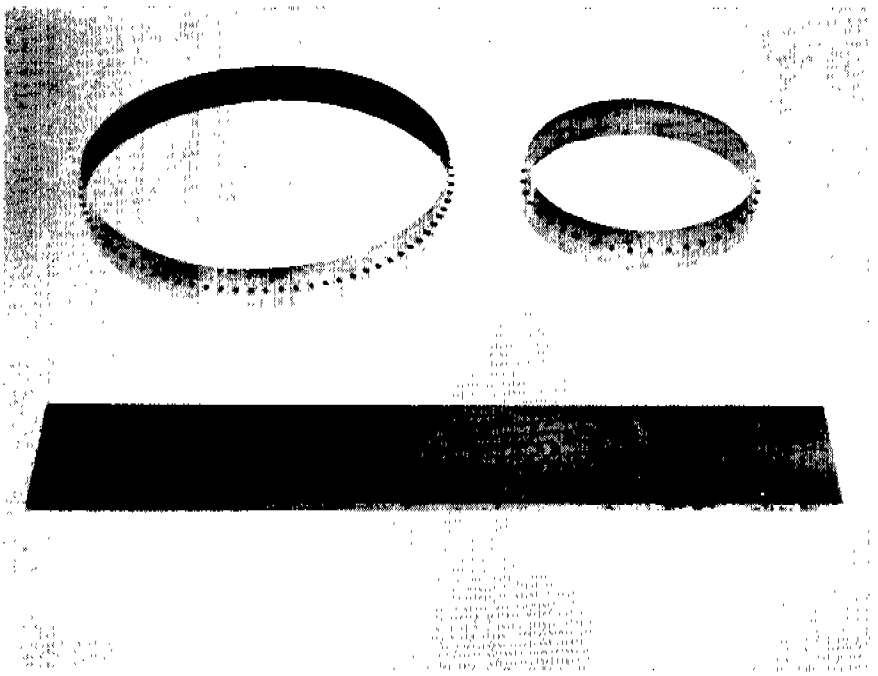

(b) BAND ROUGHNESS MOUNTING

Figure 2. Methods of Mounting Spherical Roughness Elements on Cone

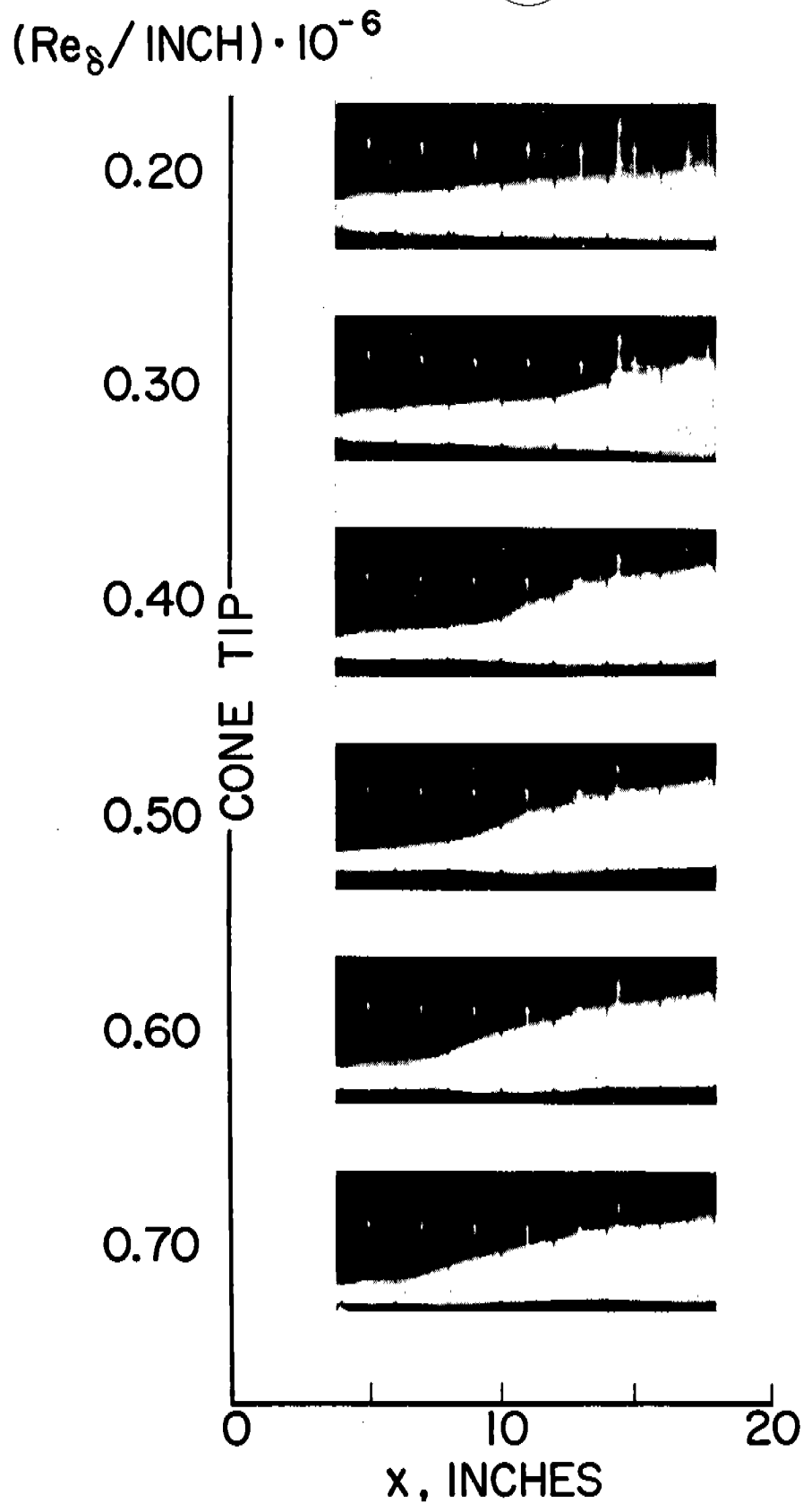

Figure 3. Typical Magnified Schlieren Photographs of Transition on Smooth Adiabatic Cone, $M_\delta = 2.71$

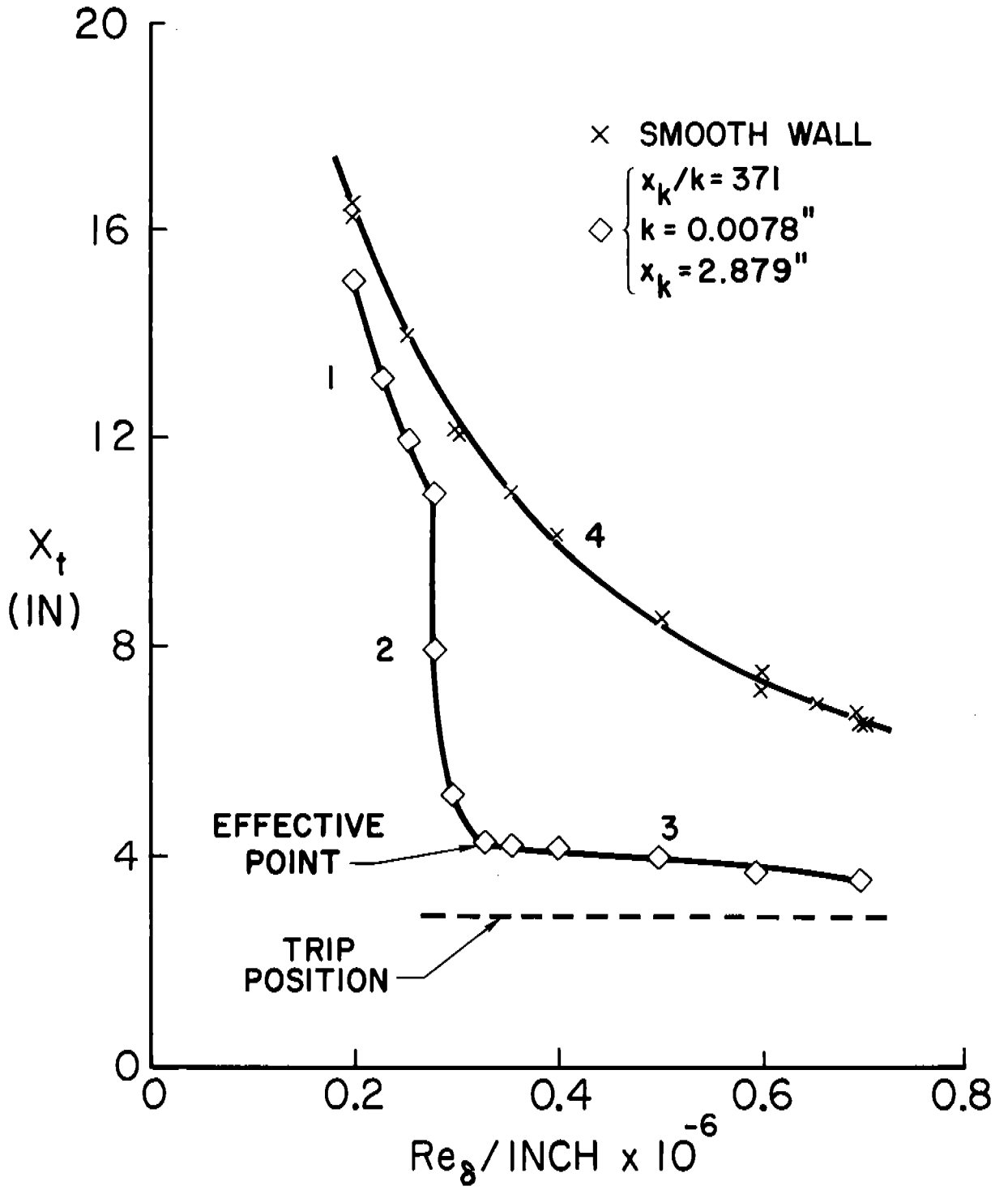

Figure 4. The Variation of Transition Location With Unit Reynolds Number on a Cone, $M_\delta = 2.71$

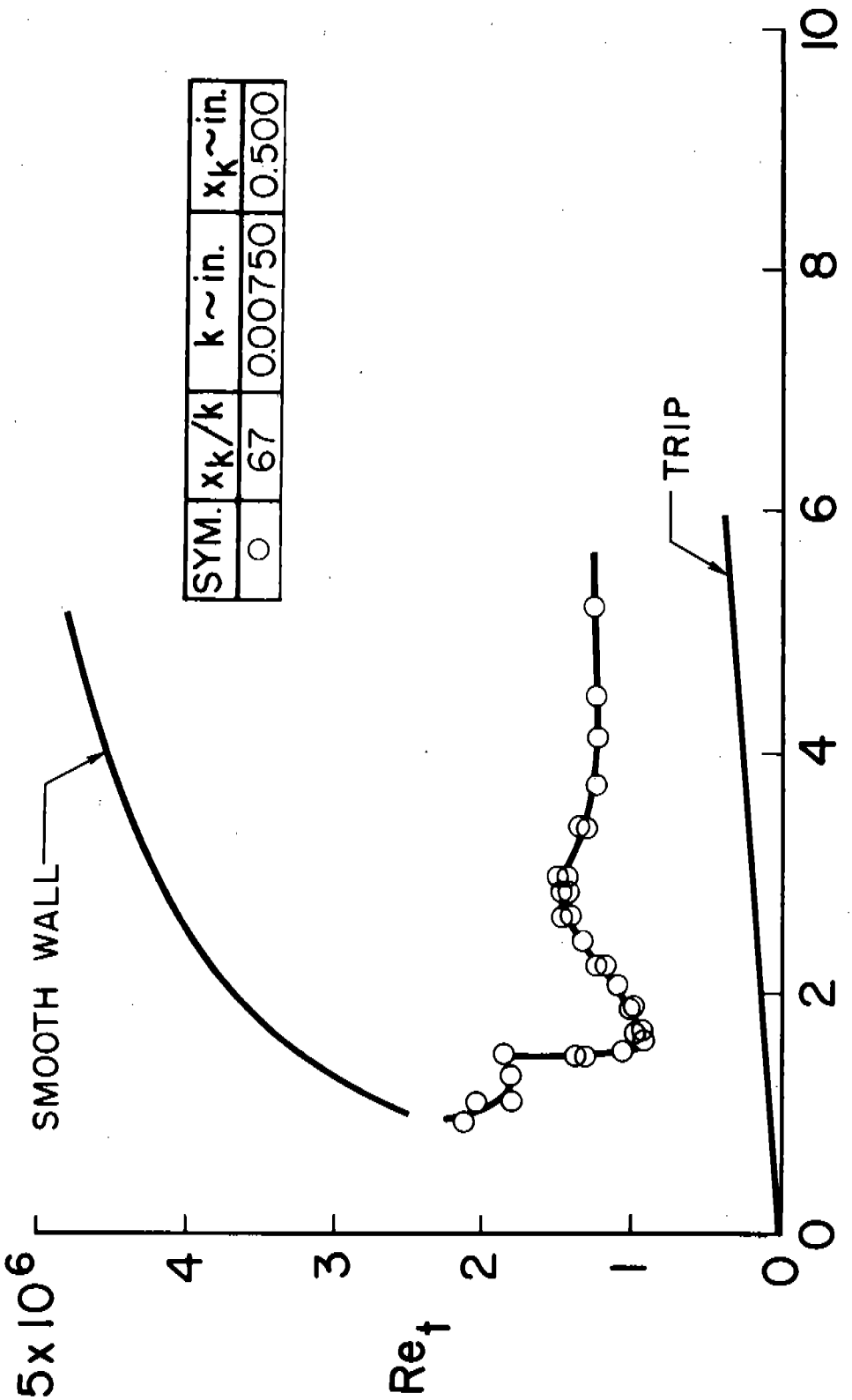

Figure 5(a). The Variation of Transition Reynolds Number With Trip Reynolds Number on a Cone, $M_\delta = 2.71$

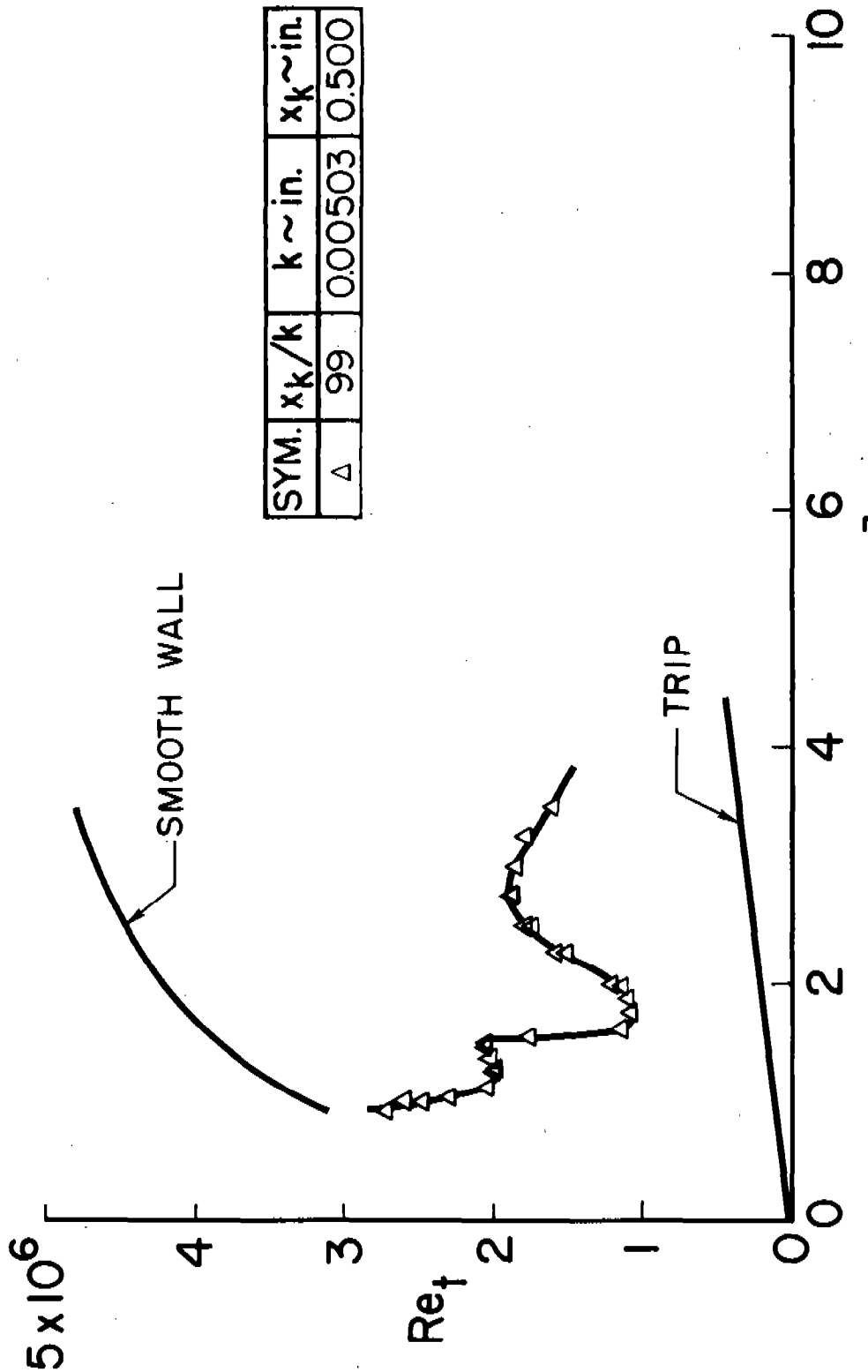

Figure 5(b). The Variation of Transition Reynolds Number With Trip Reynolds Number on a Cone, $M_\delta = 2.71$

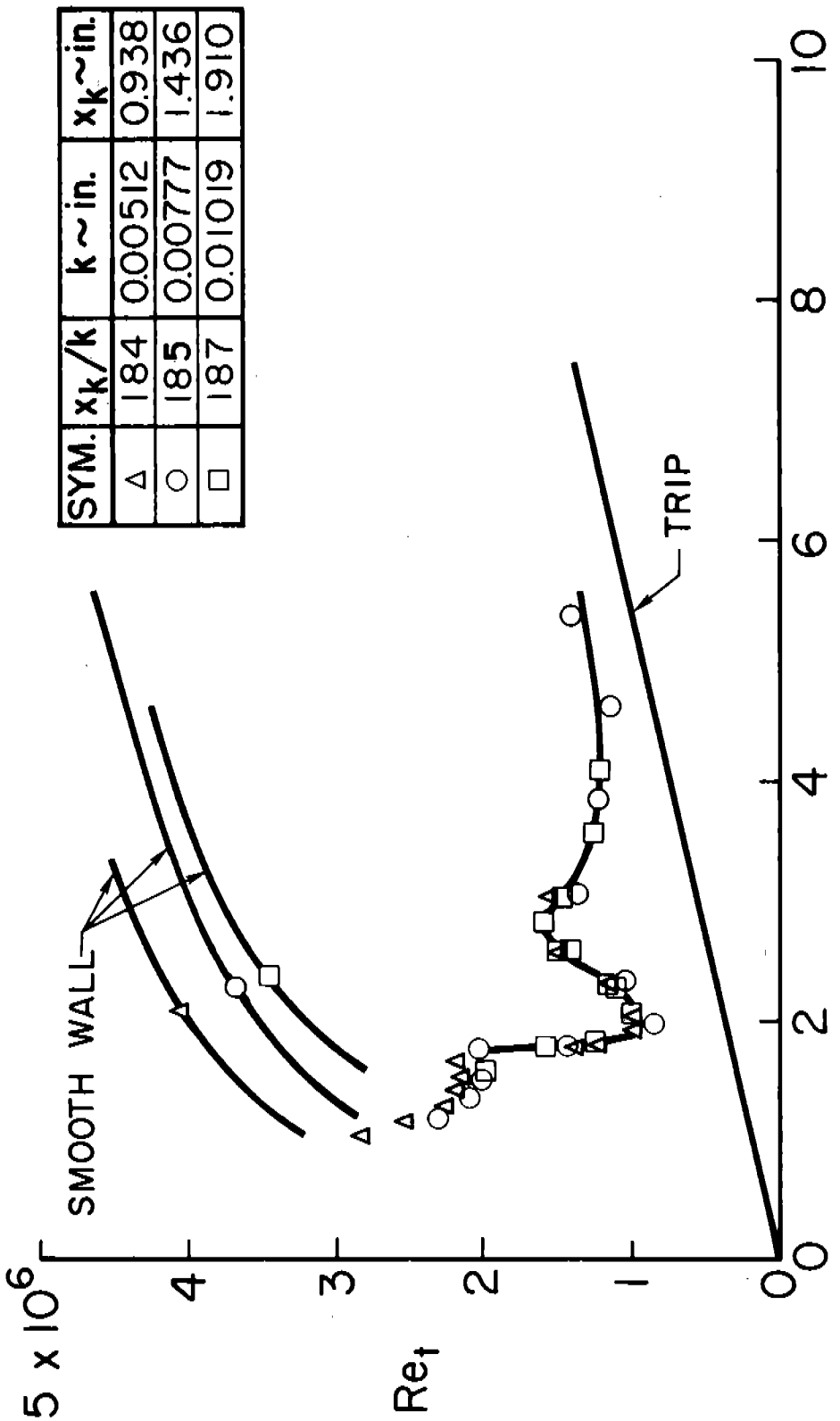

Figure 5(c). The Variation of Transition Reynolds Number With Trip Reynolds Number on a Cone, $M_\delta = 2.71$

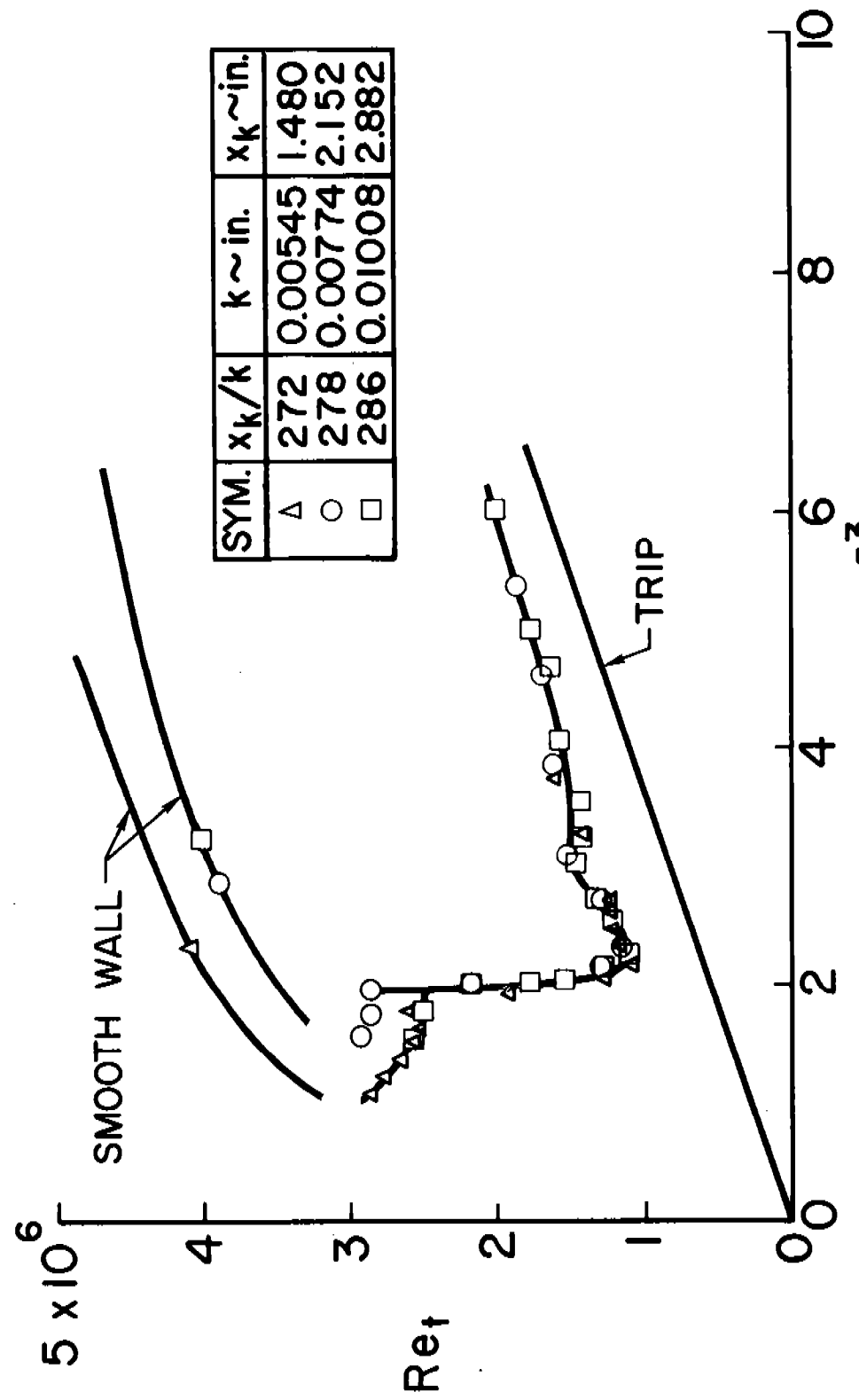

Figure 5(d). The Variation of Transition Reynolds Number With Trip Reynolds Number on a Cone, $M_\delta = 2.71$

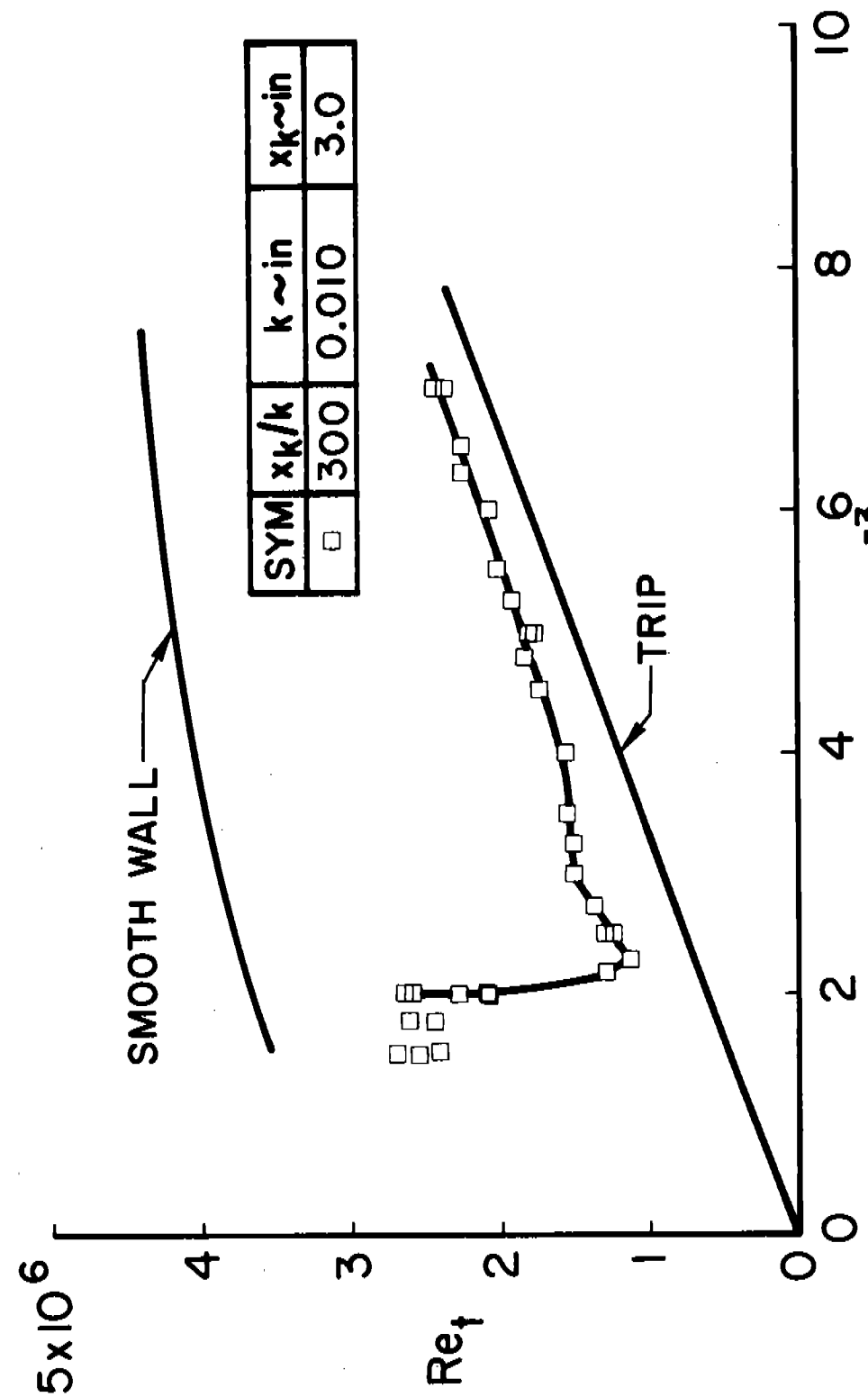

Figure 5(e). The Variation of Transition Reynolds Number With Trip Reynolds Number on a Cone, $M_\delta = 2.71$

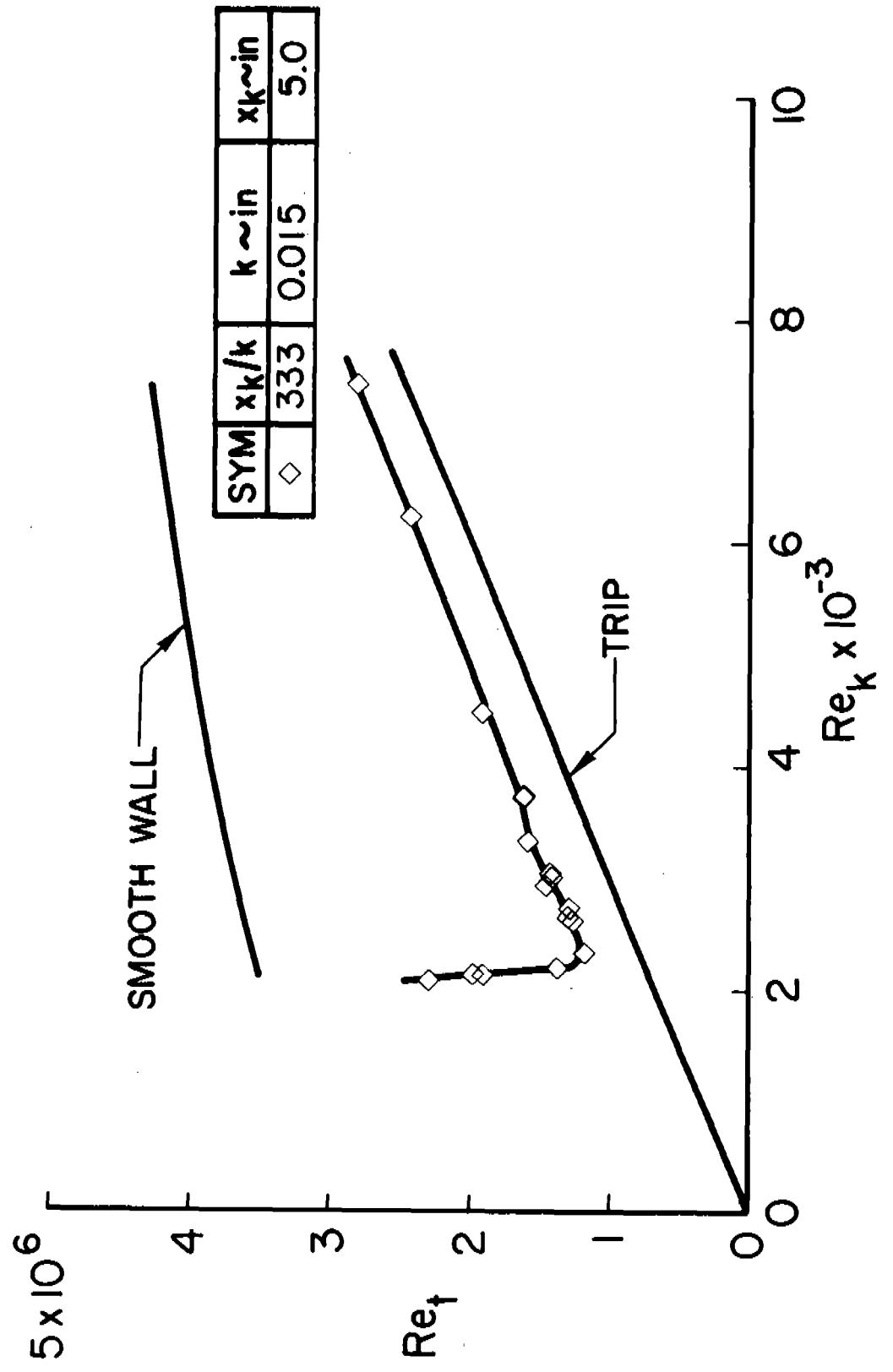

Figure 5(f). The Variation of Transition Reynolds Number With Trip Reynolds Number on a Cone, $M_\delta = 2.71$

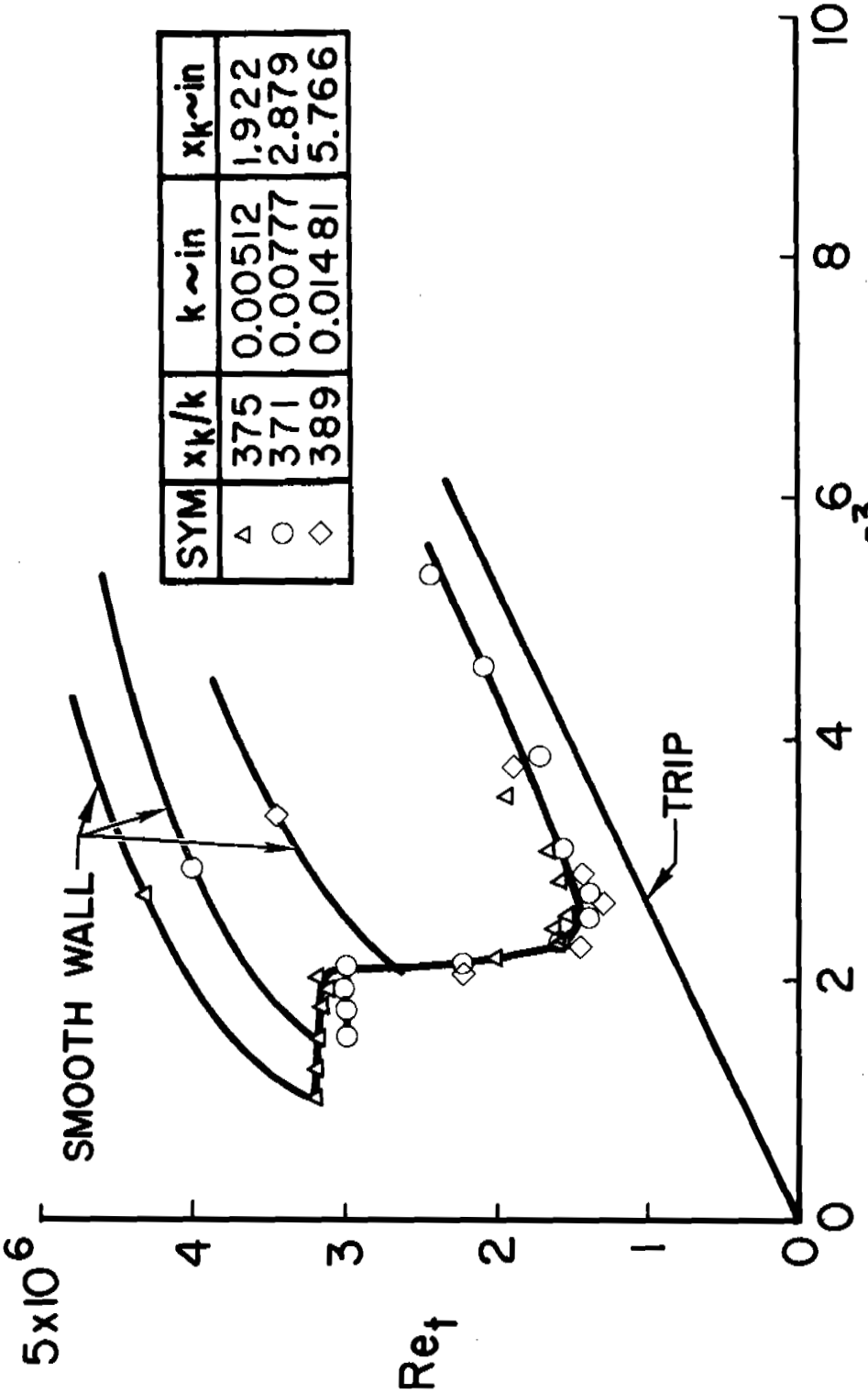

Figure 5(g). The Variation of Transition Reynolds Number With Trip Reynolds Number on a Cone, $M_\delta = 2.71$

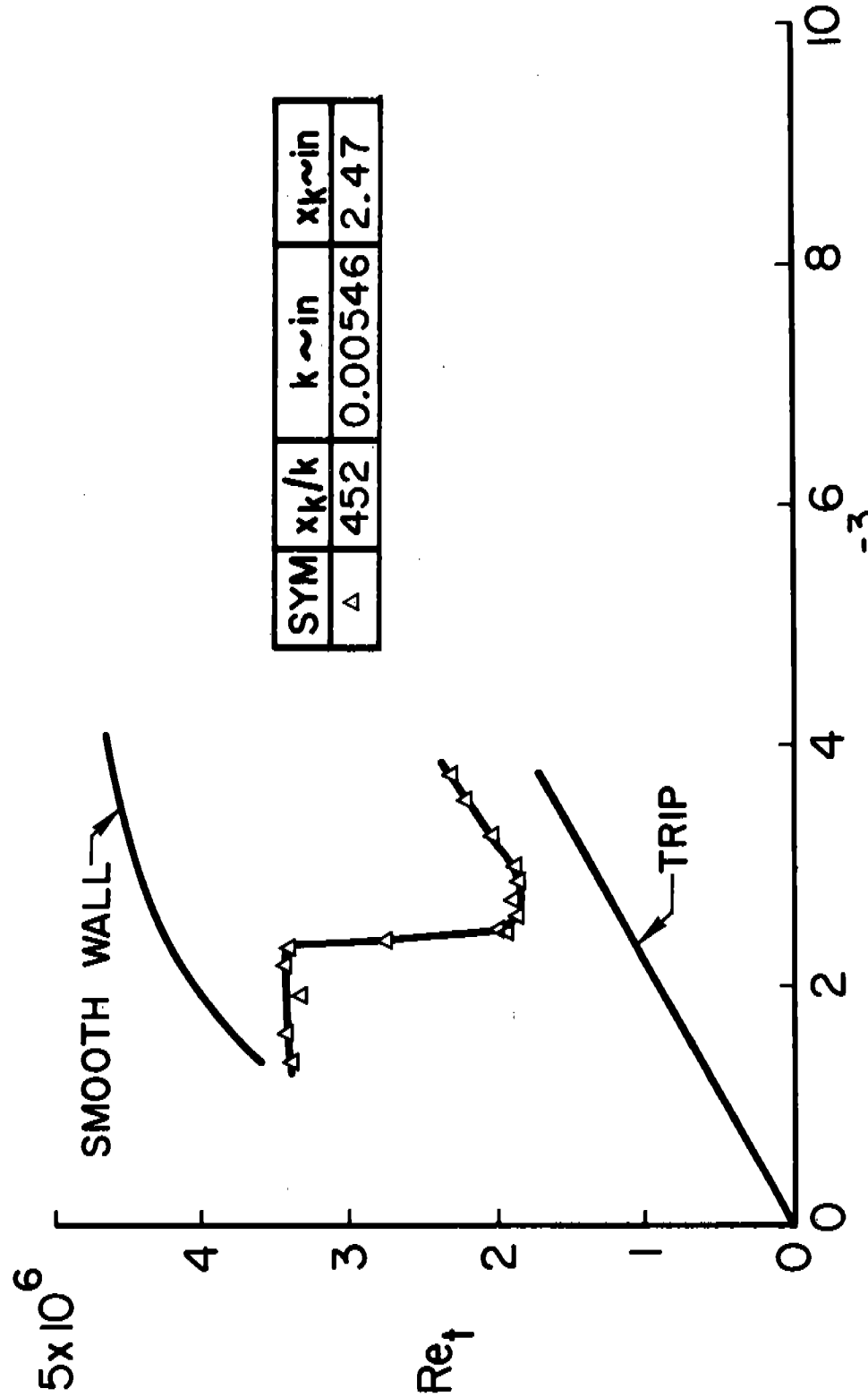

Figure 5(h). The Variation of Transition Reynolds Number With Trip Reynolds Number on a Cone, $M_\delta = 2.71$

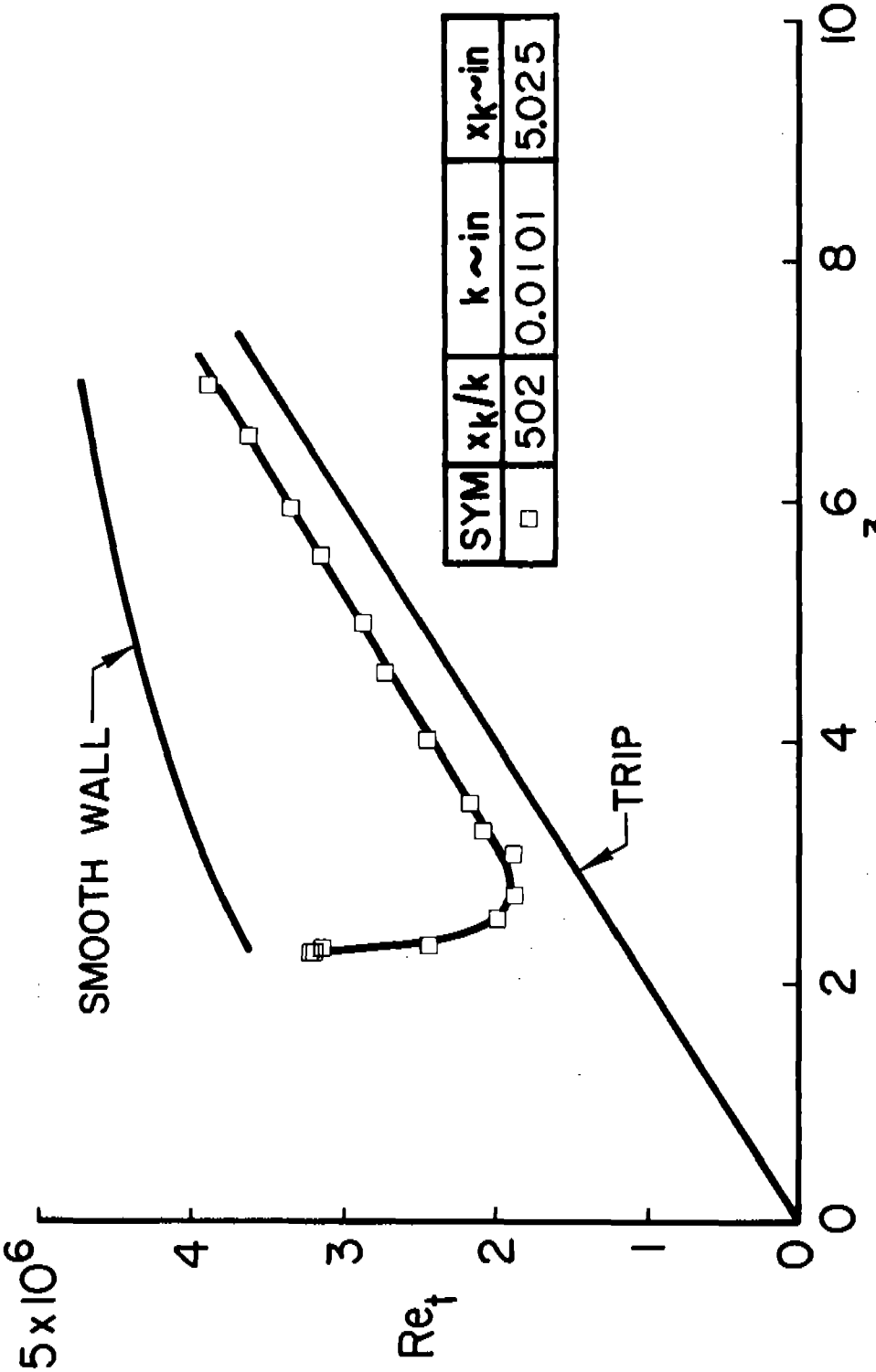

Figure 5(i). The Variation of Transition Reynolds Number With Trip Reynolds Number on a Cone, $M_\delta = 2.71$

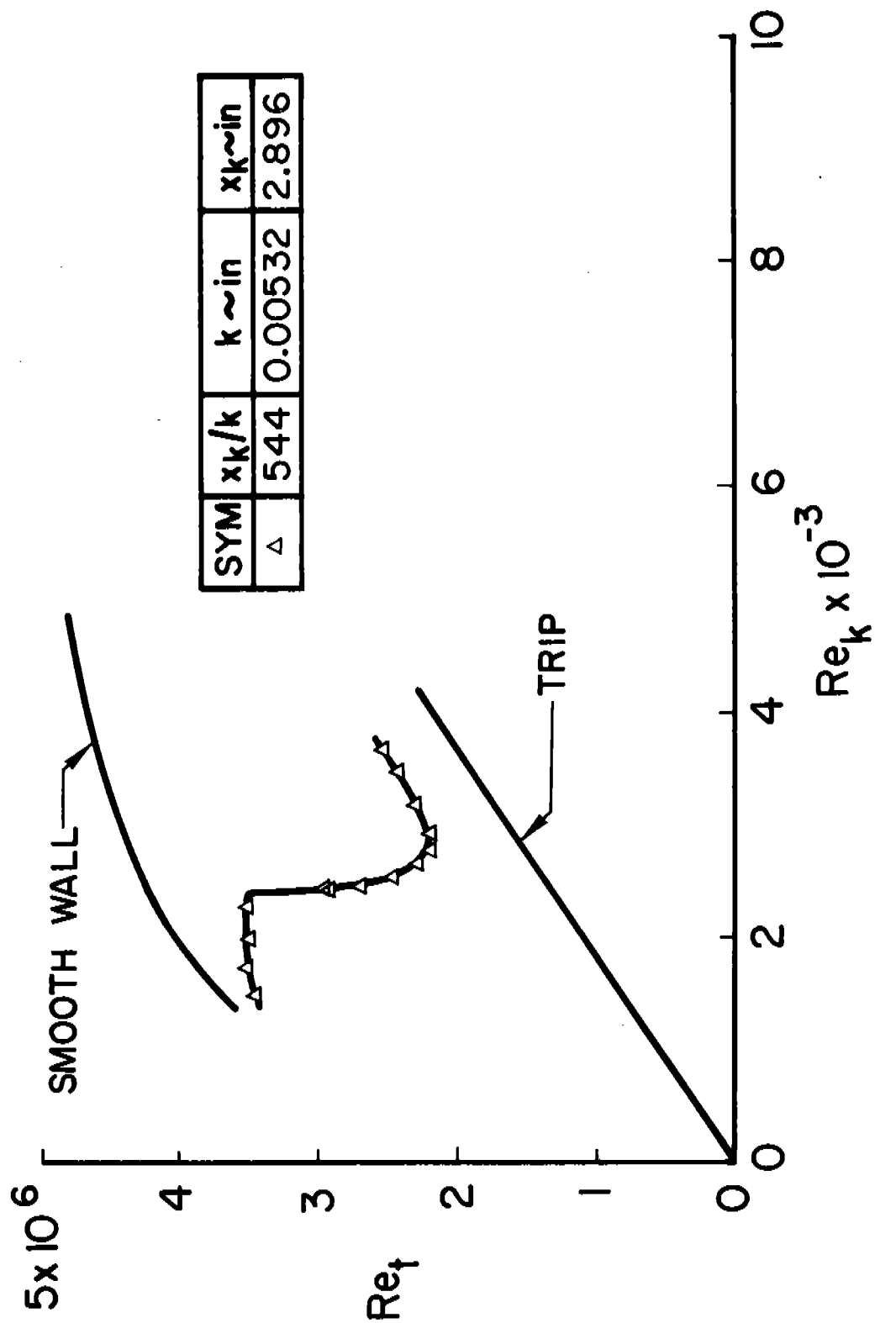

Figure 5(j). The Variation of Transition Reynolds Number With Trip Reynolds Number on a Cone, $M_\delta = 2.71$

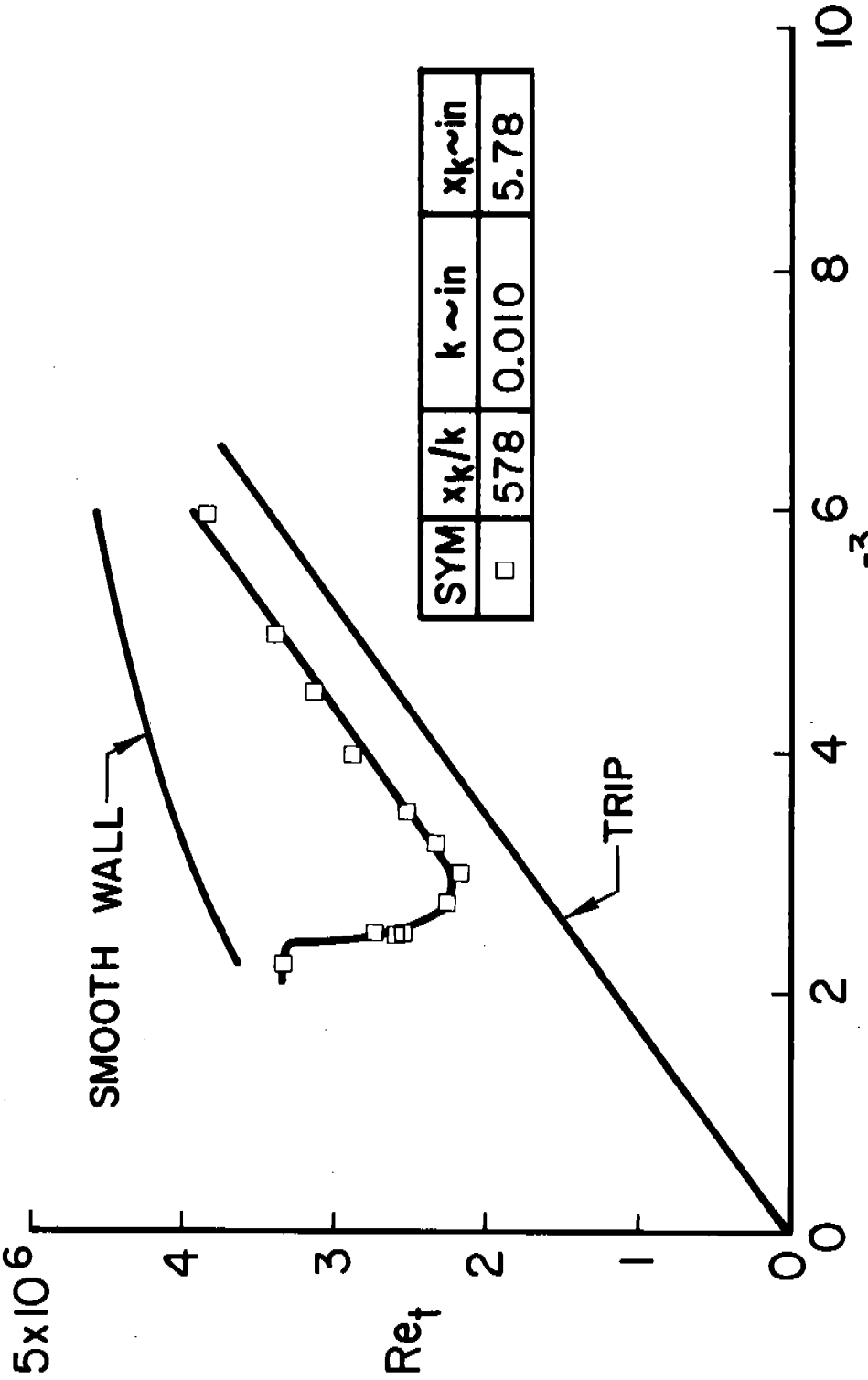

Figure 5(k). The Variation of Transition Reynolds Number With Trip Reynolds Number on a Cone, $M_\delta = 2.71$

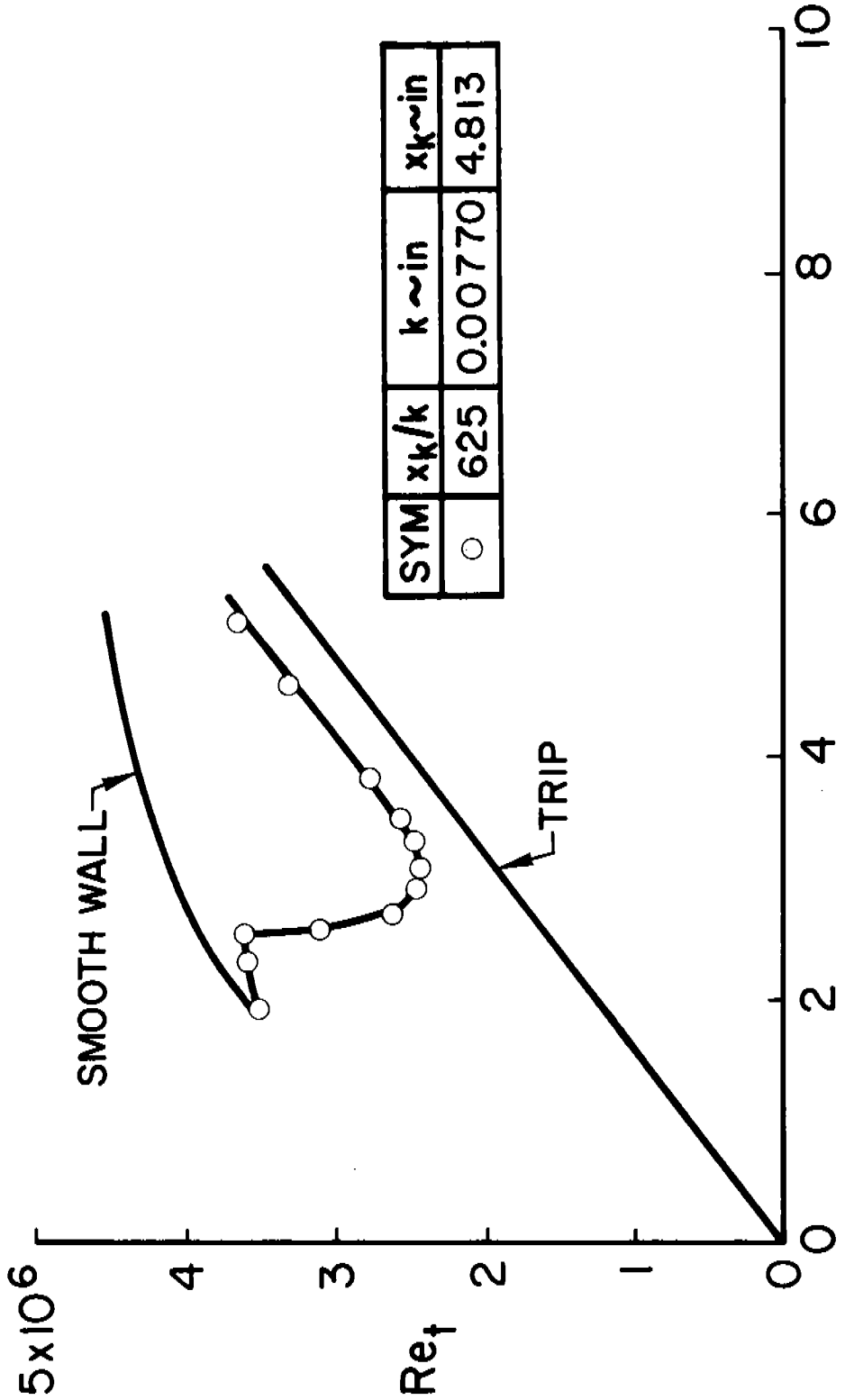

Figure 5(1). The Variation of Transition Reynolds Number With Trip Reynolds Number on a Cone, $M_\delta = 2.71$

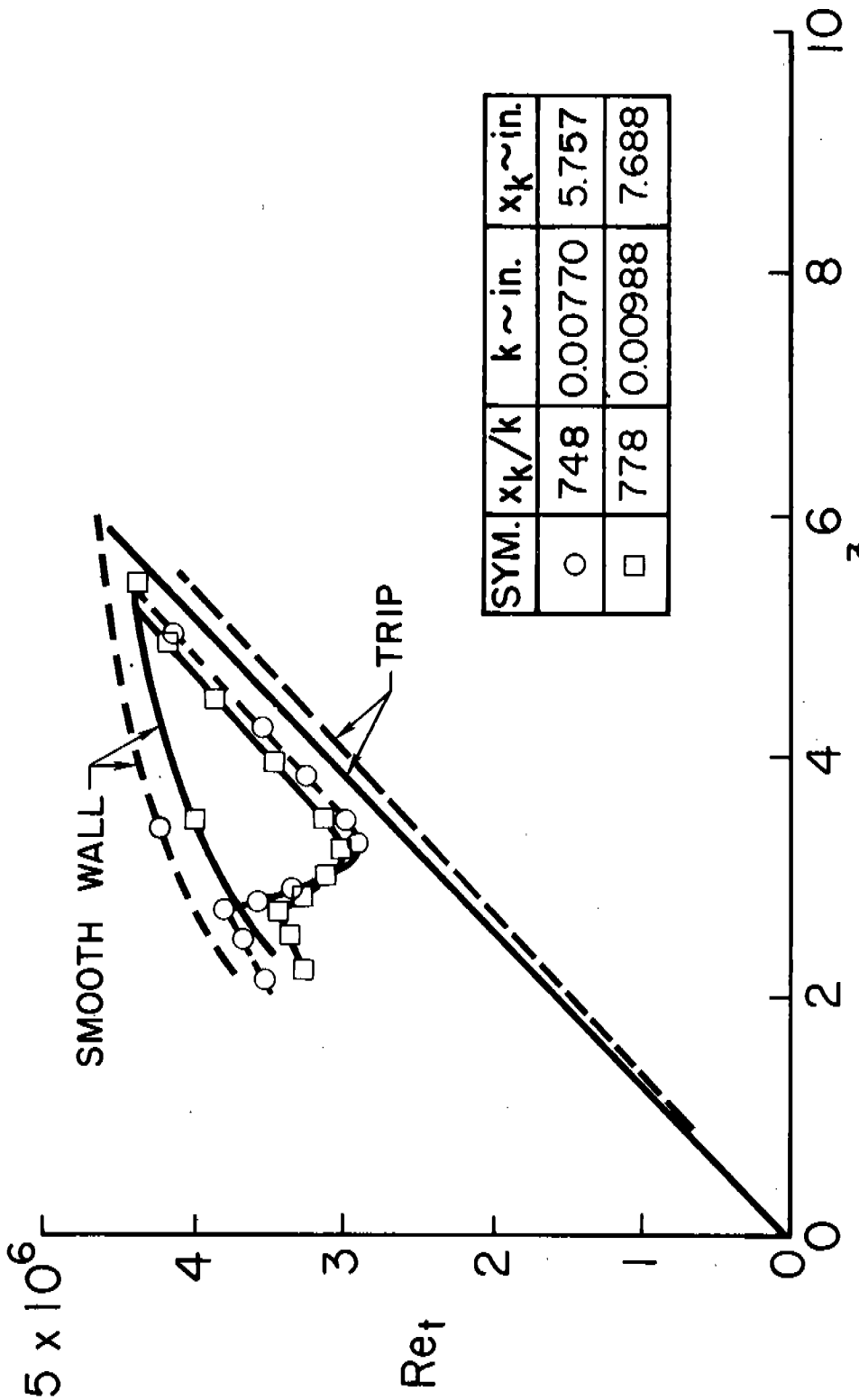

Figure 5(m). The Variation of Transition Reynolds Number With Trip Reynolds Number on a Cone, $M_\delta = 2.71$

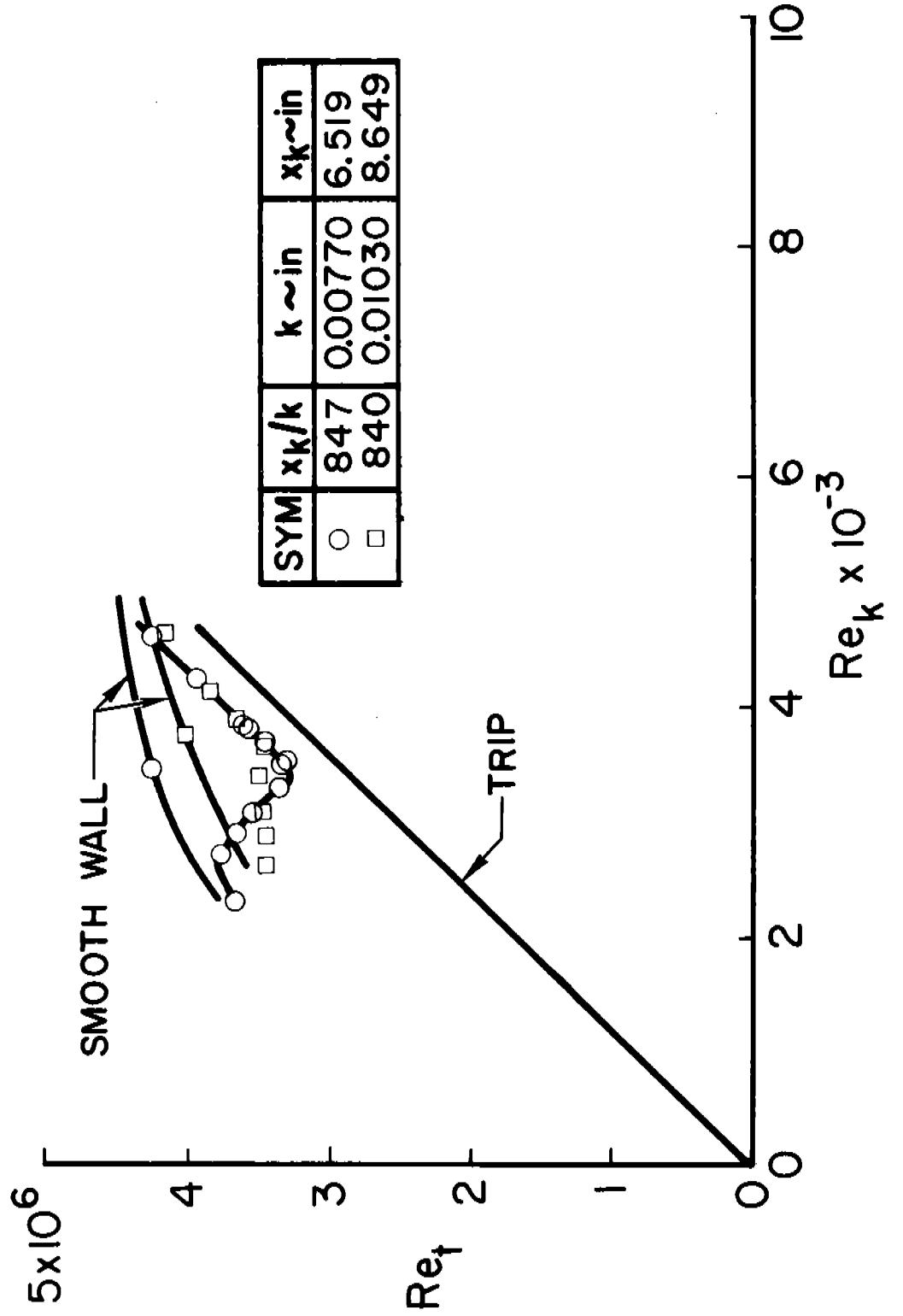

Figure 5(n). The Variation of Transition Reynolds Number With Trip Reynolds Number on a Cone, $M_\delta = 2.71$

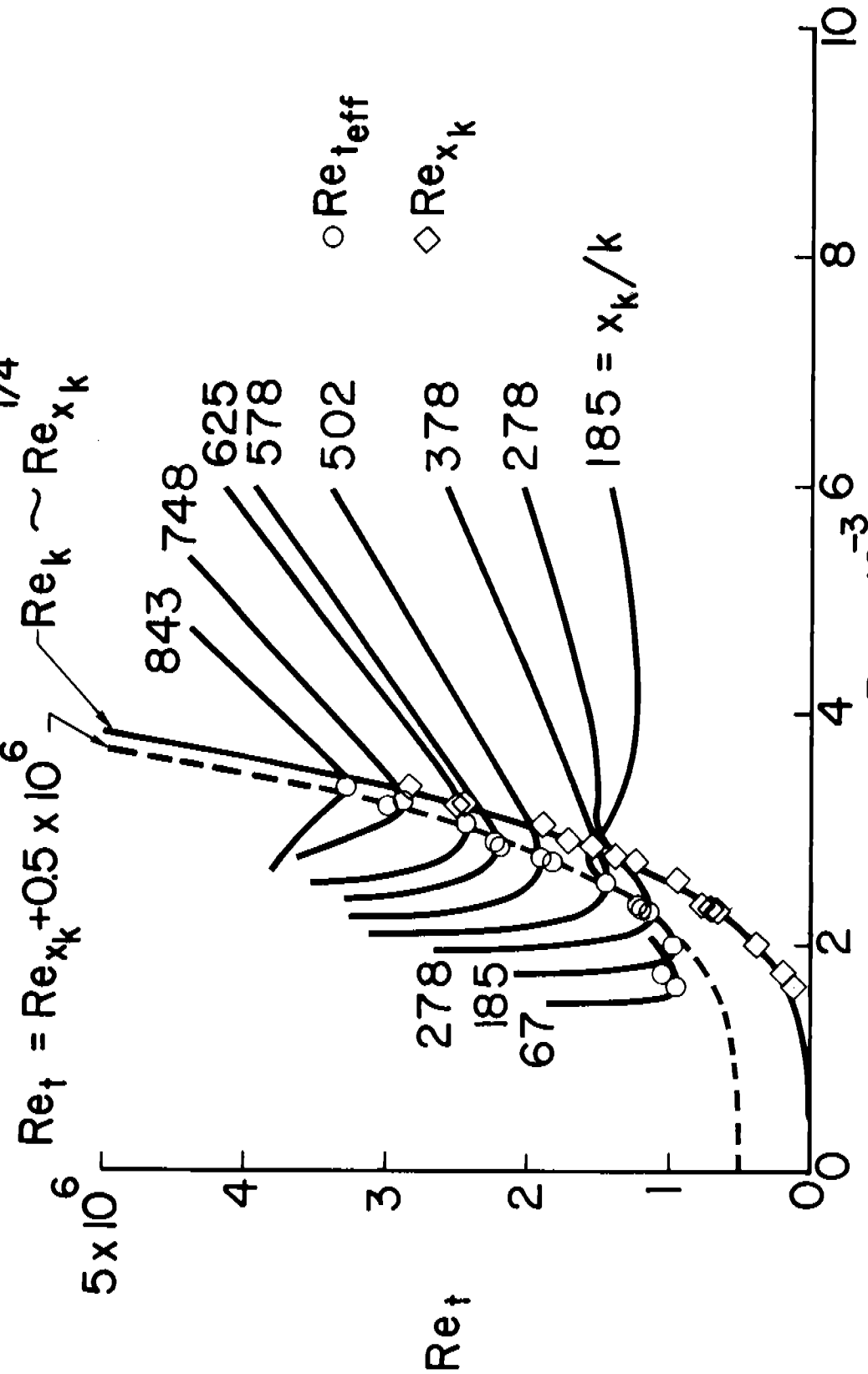

Figure 6. Summary of Roughness Induced Transition Data on a Cone $M_\delta = 2.71$

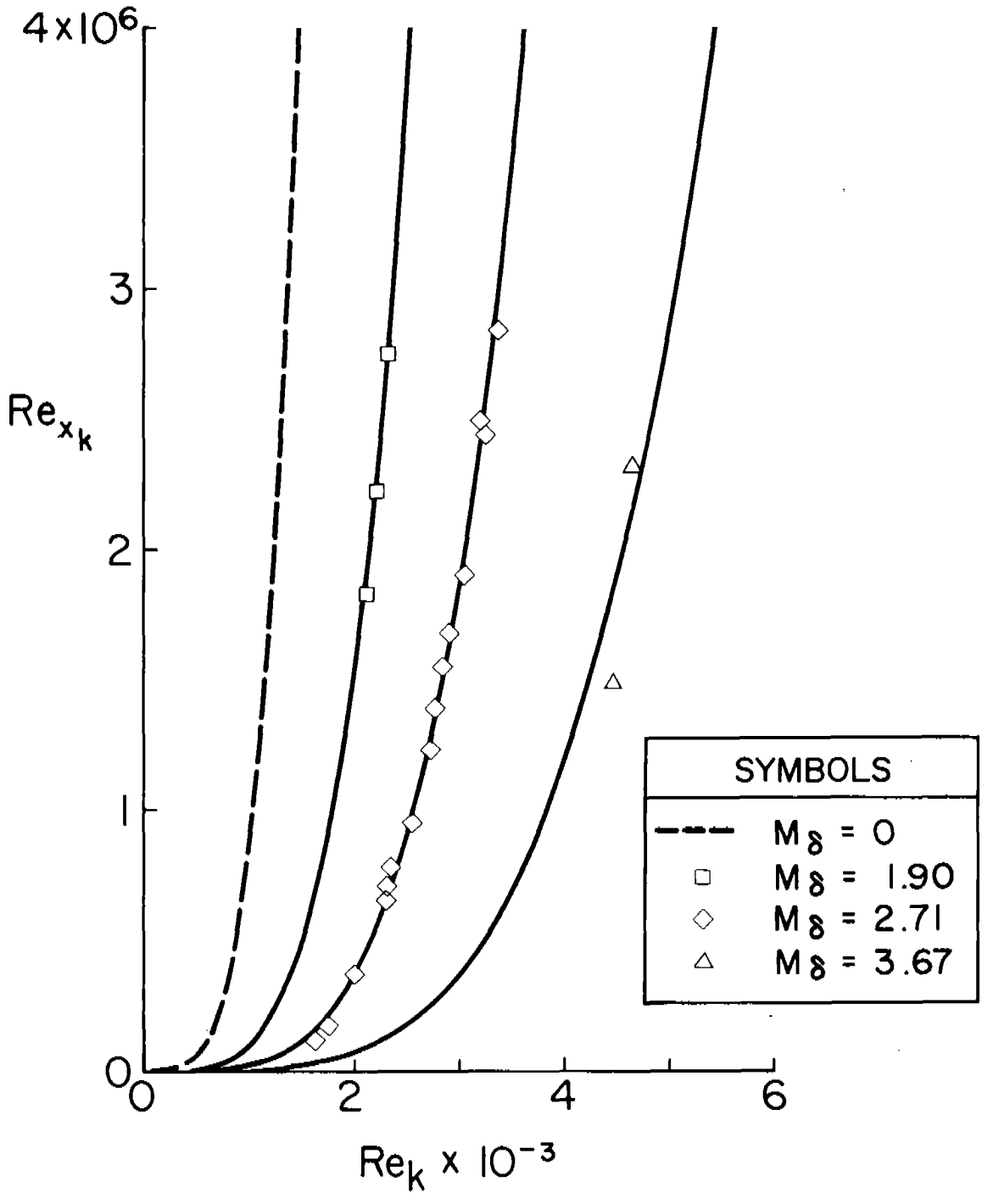

Figure 7. Effective Trip Position Reynolds Number on a Cone Versus Trip Reynolds Number for Various Mach Numbers

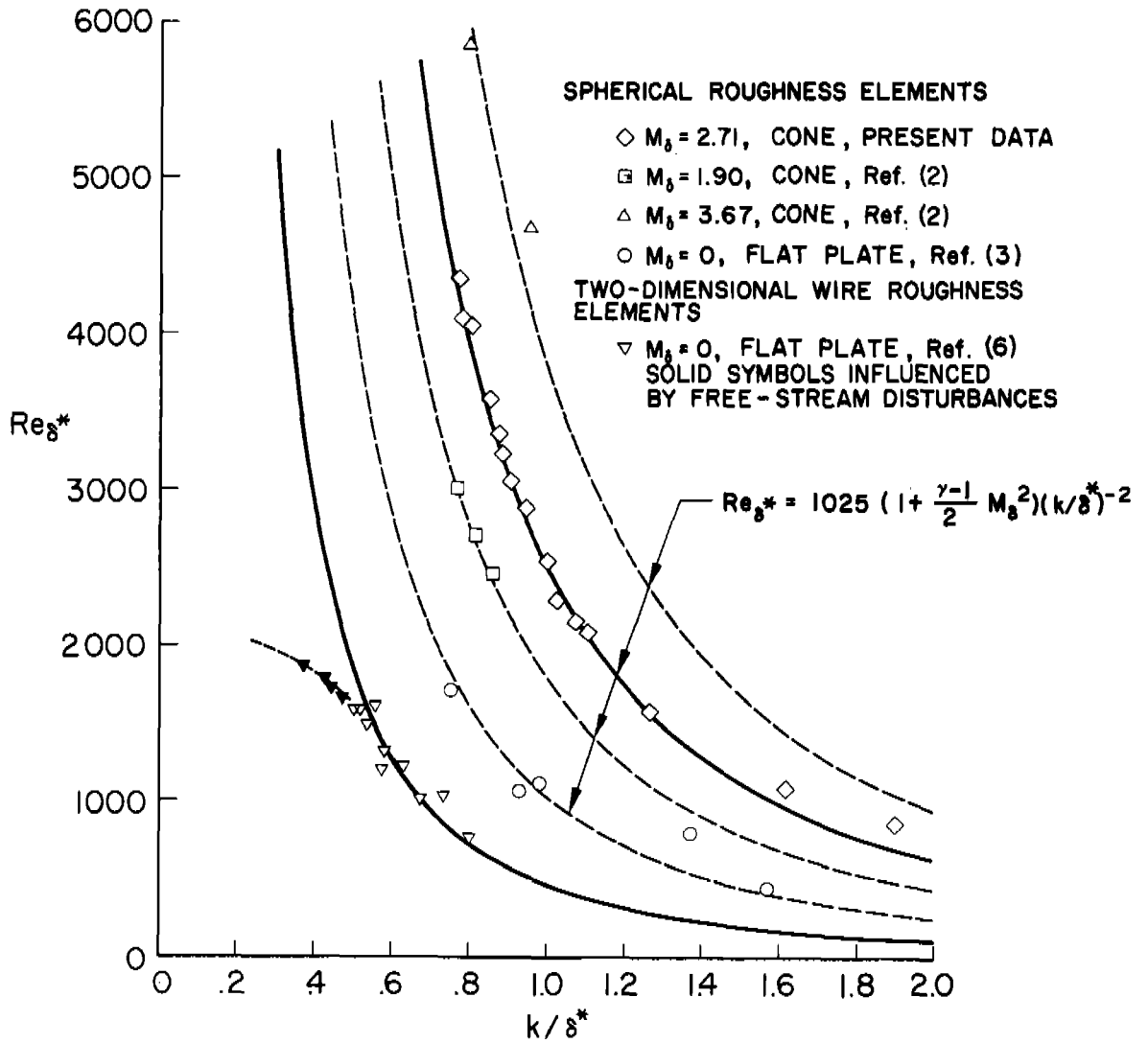

Figure 8. Effective Displacement-Thickness Transition Reynolds Number Versus k/δ^* for Various Mach Numbers

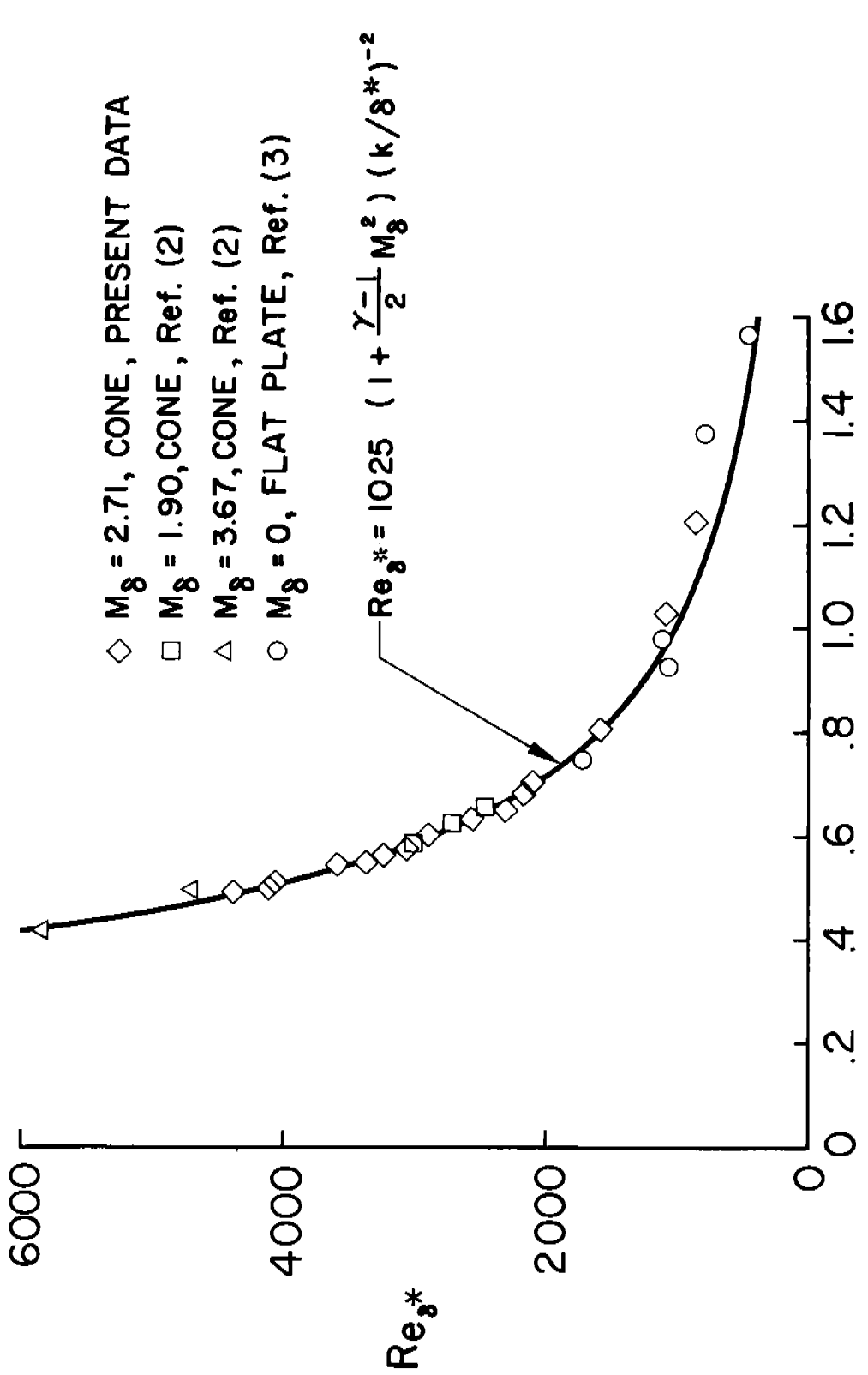

Figure 9. Composite Plot of Spherical Roughness Data for Various Mach Numbers

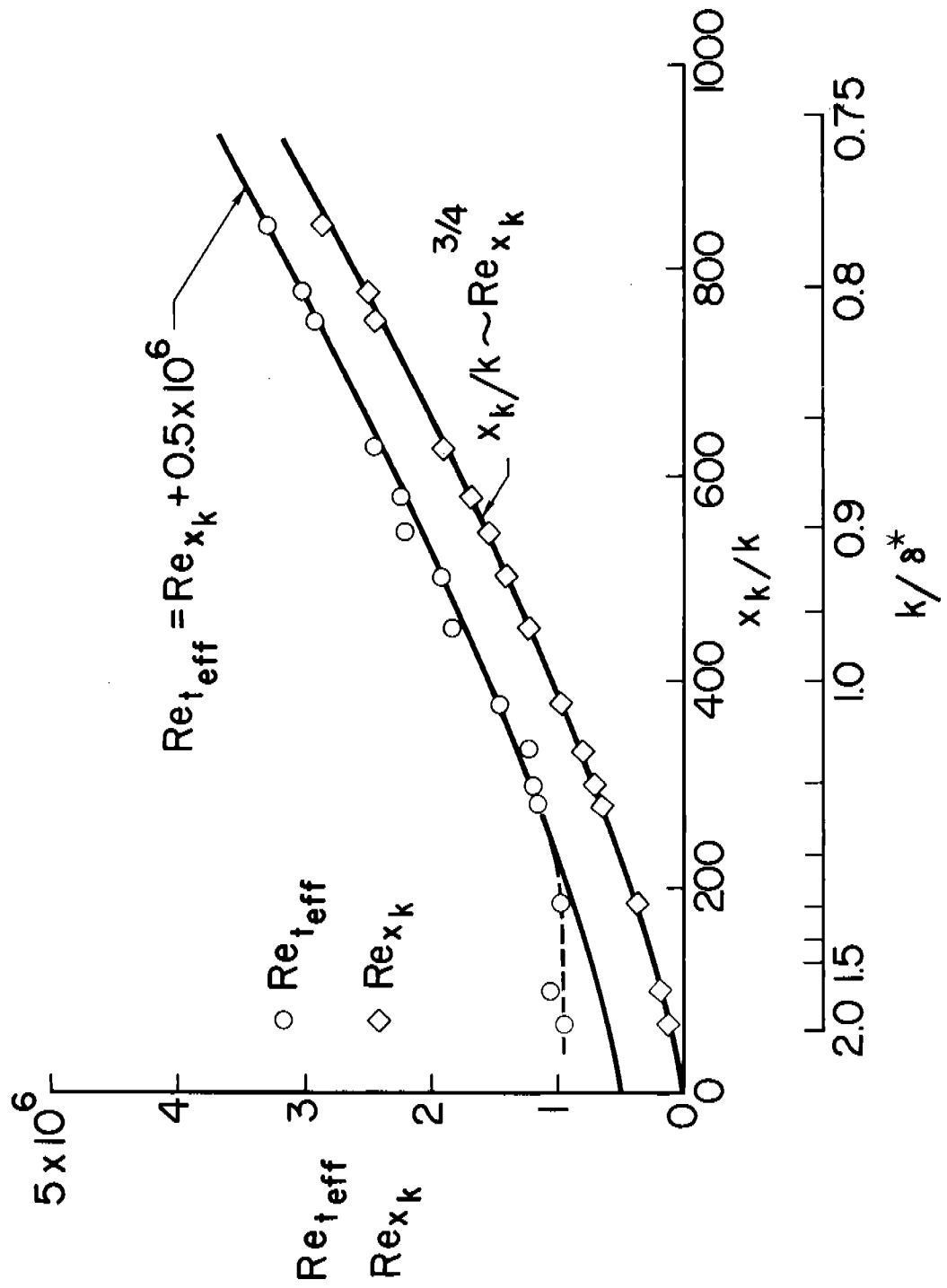

Figure 10. The Variation of Effective Transition Reynolds Number With Trip Number on a Cone, $M_\delta = 2.71$

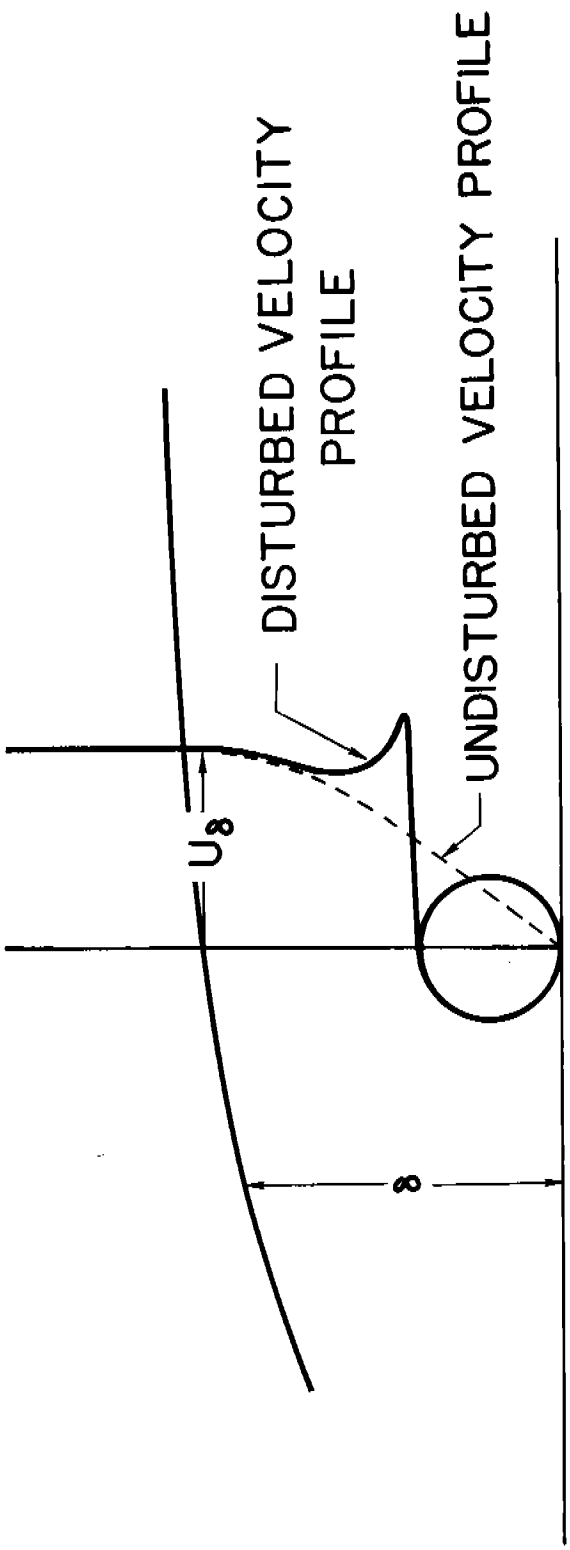

Figure 11. Schematic Diagram of the Velocity Profile in the Region of the Disturbing Element

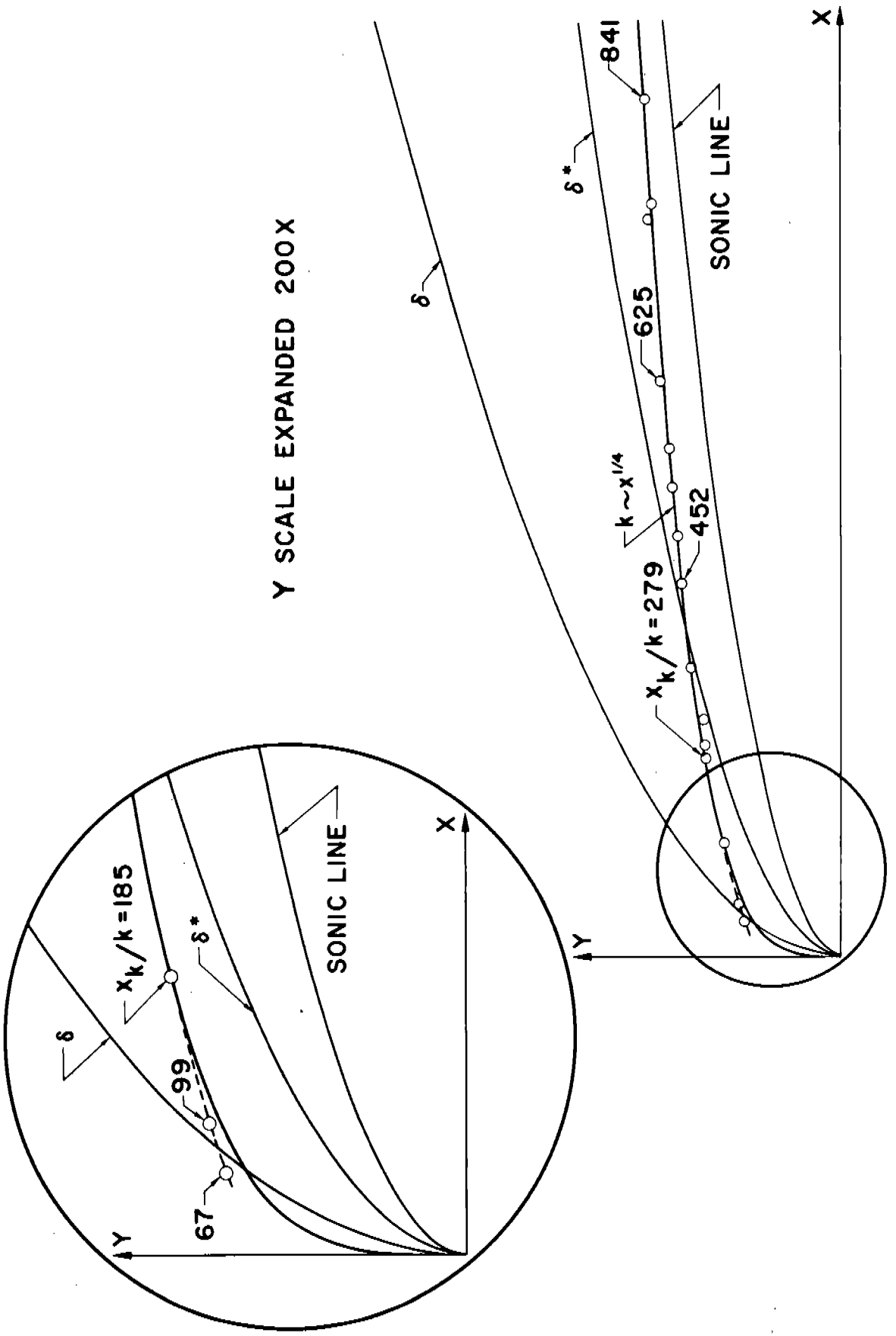

Figure 12. The Relative Height of Effective Trips in a Laminar Boundary Layer at $M_\delta = 2.71$

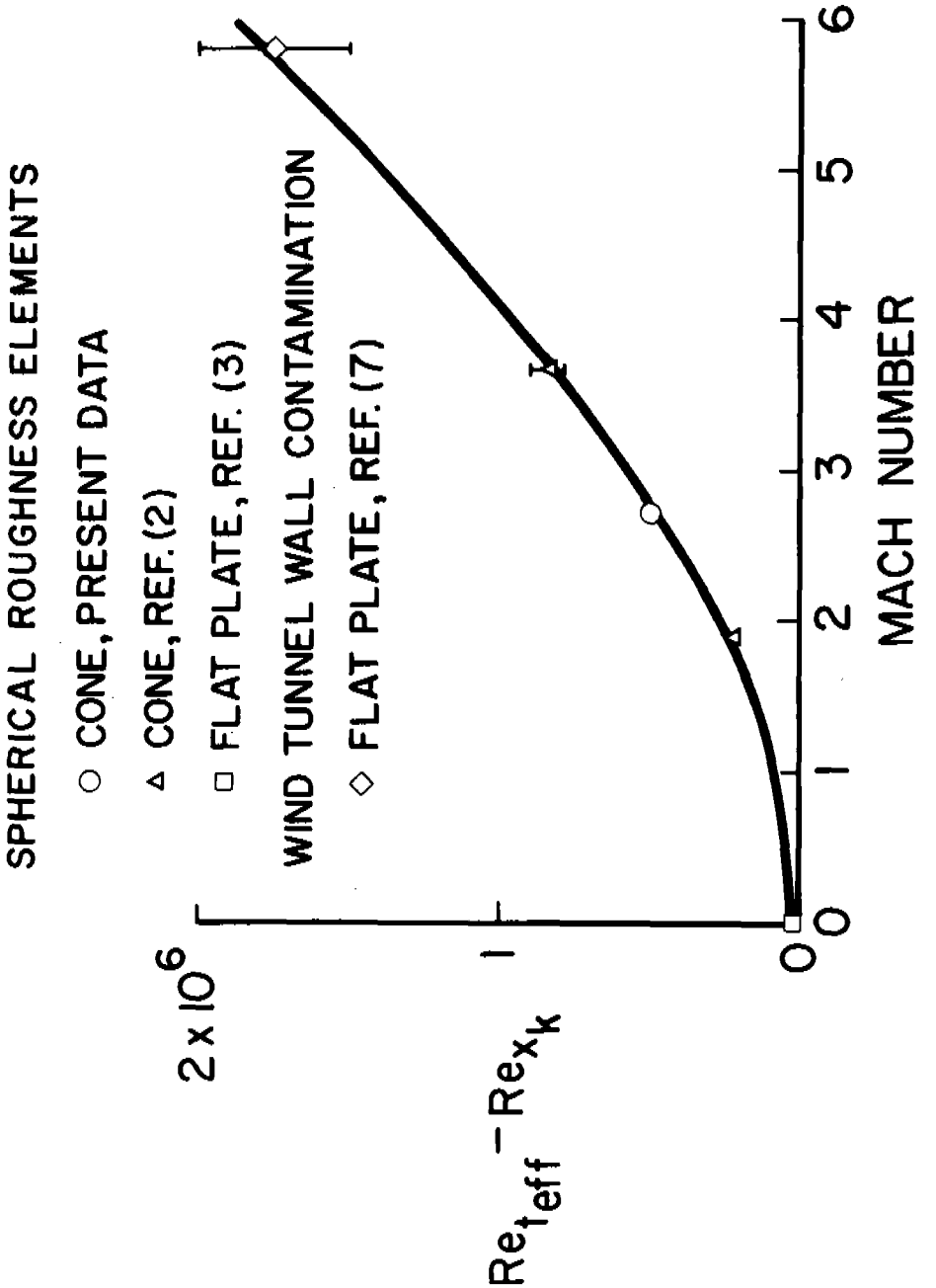

Figure 13. Interval Between Transition and Effective Roughness Elements as a Function of Mach Number

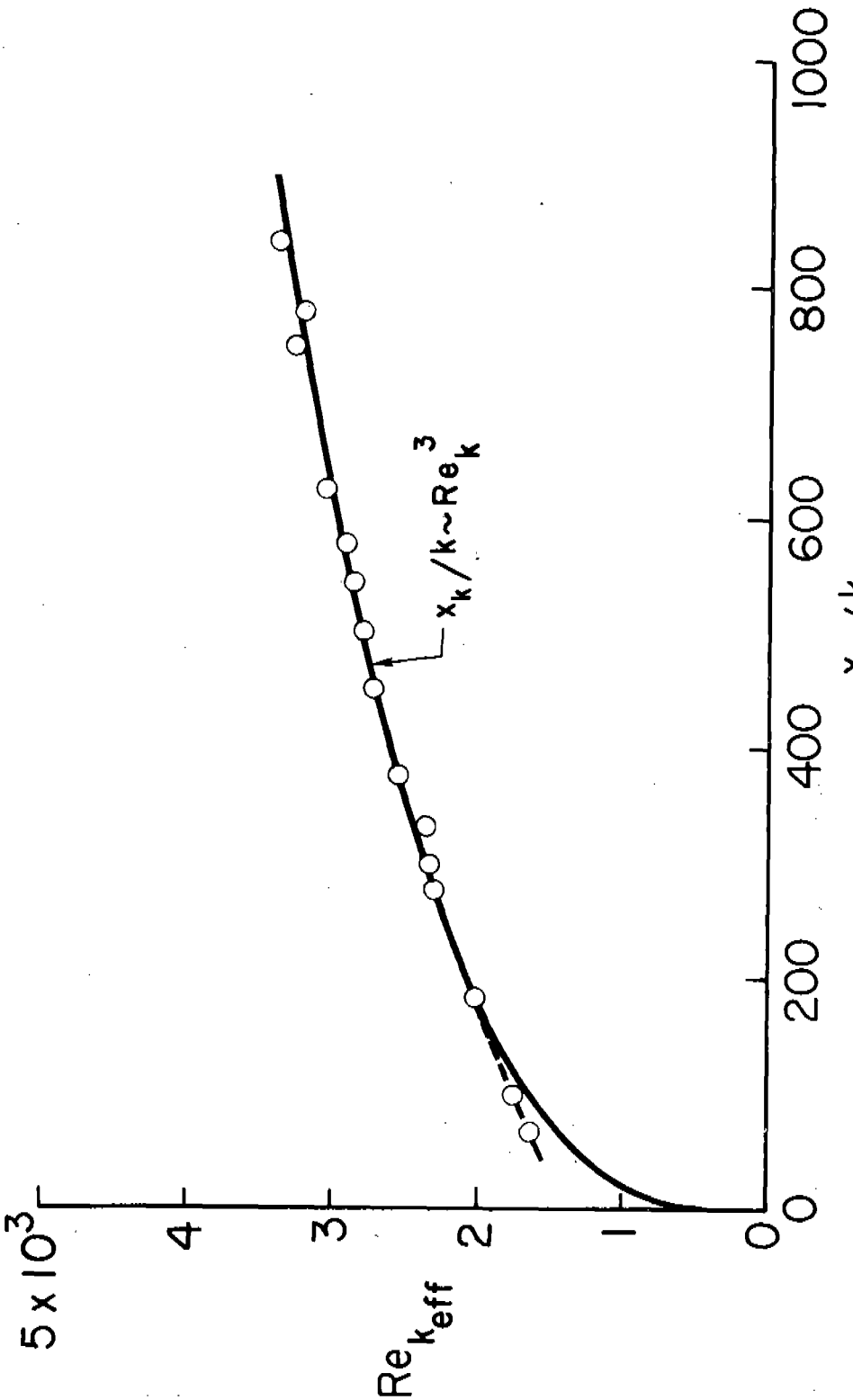

Figure 14. The Variation of Effective Trip Reynolds Number With Trip Number on a Cone, $M_\delta = 2.71$